Title
JEFFREY-HAMEL FLOW OF LESLIE-ERICKSEN NEMATIC LIQUIDS

Authors
Rey, A.D.
Denn, M.M.

Publication Date
1987-07-01

LBL-23828
Preprint

Center for Advanced Materials

CAM REPORT

Submitted to Journal of Non-Newtonian Fluid Mechanics

Jeffrey-Hamel Flow of Leslie-Ericksen Nematic Liquids

A.D. Rey and M.M. Denn

July 1987

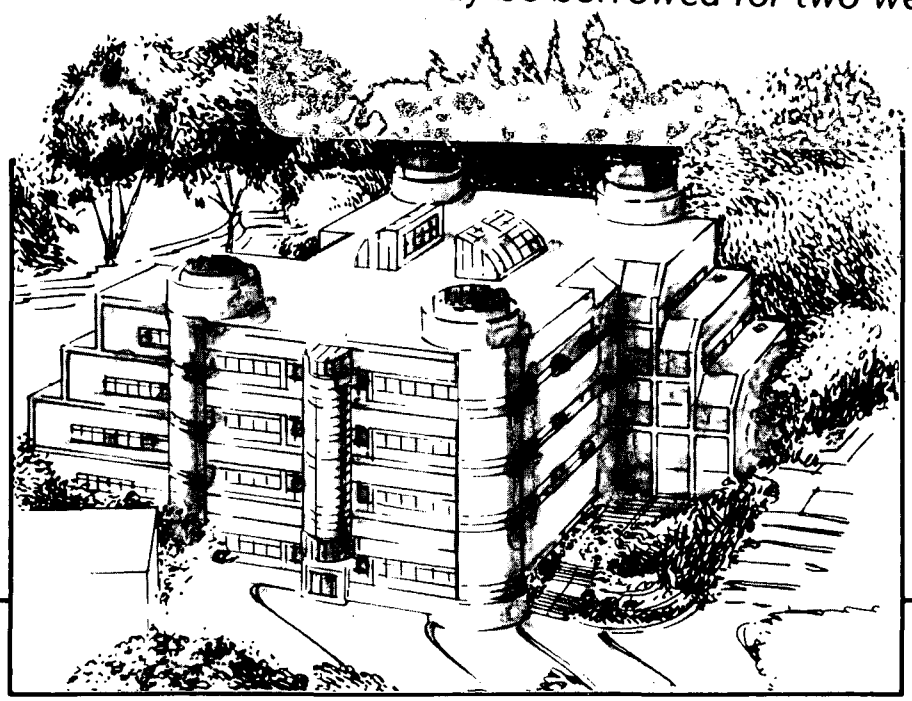

Materials and Chemical Sciences Division

Lawrence Berkeley Laboratory • University of California

ONE CYCLOTRON ROAD, BERKELEY, CA 94720 • (415) 486-4755

Prepared for the U.S. Department of Energy under Contract DE-AC03-76SF00098

DISCLAIMER

July 9, 1987

For submission to J. Non-Newtonian Fluid mechanics

JEFFREY-HAMEL FLOW OF LESLIE-ERICKSEN NEMATIC LIQUIDS

Alejandro D. Rey and Morton M. Denn

Center for Advanced Materials, Lawrence Berkeley Laboratory

and

Department of Chemical Engineering, University of California

Berkeley, CA 94720 USA

Summary

A similarity solution of the Leslie-Ericksen equations for nematic liquid crystals is obtained for flow between converging and diverging planar walls (Jeffrey-Hamel flow). There are three regions in the flow:extensional or compressional flow near the centerline, shear near the wall, and a wall boundary layer in which elastic stresses control the transition from the wall-induced orientation to the bulk behavior. The boundary layer thickness is obtained in closed form; the scaling with the Ericksen number depends on whether or not the boundary layer extends into the region of extensional flow. Imposition of a magnetic field with an azimuthal component in a converging flow can result in a Freedericksz-like transition from radial to transverse orientation at the center line at a critical field strength. This transition provides a new means to measure the irrotational viscosity λ_2.

I. Introduction

The development of liquid crystalline polymers has led to a renewed interest in the mechanics of nematic liquids. A complete dynamical continuum theory of nematic liquid crystals has been proposed by Leslie [1,2], building on Ericksen's [3] theory of the Transverseley Isotropic Liquid and the Oseen [4] – Frank [5] theory of liquid crystalline elasticity; see the book by deGennes [6], for example. There is a nice discussion of the Leslie-Ericksen theory in a lecture by Ericksen [7], and Leslie [8] and Jenkins [9] have reviewed the theory and solutions to flow problems. More recent analyses of flows of nematic liquid crystals have been carried out by Carlsson [10].

Liquid crystals can be aligned at a solid boundary, and the boundary alignment might differ from the alignment induced by flow; one of the prominent characteristics of the flow is therefore the development of an orientation boundary layer, in which the magnitude of the elastic stresses controls the spatial transition. A second characteristic of these liquids is their orientability in an electro-magnetic field; the competition between wall alignment and alignment by the external field in a static nematic liquid leads to a "Freedericksz transition" and the creation of another type of orientation boundary layer. Finally, for certain values of the rheological parameters there is a transition to a "tumbling" state of orientation, in which rapid changes of orientation are observed across the flow field.

Studies of the flow of nematic liquid crystals have emphasized viscometric geometries. The only fluid mechanical analyses of non-viscometric flows of a Leslie-Ericksen fluid have been restricted to the

special case of the Transversely Isotropic Liquid (*TIL*); Leslie [11] has obtained a similarity solution for converging or diverging flow between planar walls (*Jeffrey-Hamel flow*), and Vanderheyden and Ryskin [12] have described numerical solutions for converging and diverging geometries. Evans [13] and Lipscomb and coworkers [14] have reported numerical solutions of converging flow for a theory of dilute fiber suspensions that is equivalent to a statistical averaging of the TIL equations over initial orientation distributions. The TIL equations do not include the nematic elasticity, and hence these solutions cannot accomodate wall-induced orientation and the various boundary layer and transition phenomena that characterize liquid crystals.

The extent to which the Leslie-Ericksen (*L-E*) theory describes the behavior of nematic liquid crystalline polymers is unclear, since the full range of behavior of this constitutive theory has not been fully explored. The dynamical terms in the theory arise as the low-deformation rate limit of Doi's theory of liquid crystalline polymers [Doi and Edwards, 15], but the Doi theory contains no analog of the Oseen-Frank elasticity and cannot be applied to flows containing elastic boundary layers. The magnetic field experiments of Moore and Denn [16] show that the Oseen-Frank elasticity in some thermotropic liquid crystal polymers can creep, and that a viscoelasticity that is dependent on orientation gradients must be included. It is clearly essential to define the full scope of the behavior of the L-E theory, with particular emphasis on the non-viscometric flows that are of interest in processing applications.

In this paper we obtain a steady in-plane similarity solution to Jeffrey-Hamel flows of nematic liquid crystals using the L-E continuum theory. The results are restricted to rheological parameters for which

tumbling cannot occur. Several new phenomena are observed because of the interaction of center-line extension or compression, wall-region shear, and wall-induced orientation. The dependence of the orientation boundary layer on dimensionless flow rate (*Ericksen number*) changes functional form, depending on whether the shear or extensional components of the flow dominate in the boundary layer; the boundary layer results can be obtained in closed form through an asymptotic analysis. Imposition of an inhomogeneous magnetic field can cause a flow reversal. An azimuthal magnetic field can induce a new Freedericksz-like transition in orientation during flow; this transition should provide a straightforward means of measuring one of the viscosity coefficients in the continuum theory.

II. Theory and Balance Equations

The average local orientation of rigid molecules is described in the Leslie-Ericksen continuum theory by a unit vector $\underline{n}$, called the *director*. The theory allows for a microstructure with an internal angular momentum, and hence the required balance equations, using cartesian tensor notation, are

$$\rho \dot{v}_i = F_i + t_{ji,j} \tag{2.1}$$

and

$$0 = G_i + g_i + \pi_{ji,j} \tag{2.2}$$

The fluid is assumed to be incompressible. ρ is the density, and the superposed dot ($\dot{}$) denotes the material time derivative The inertia of the director is neglected. The mechanical quantities appearing in the theory are defined as follows:

F_i = external body force per unit volume

G_i = external director body force per unit volume

t_{ji} = stress tensor

π_{ji} = intrinsic director surface stress tensor

g_i = intrinsic director body force.

The constraints of incompressibility and constant director length introduce indeterminancies into the stress tensor and the intrinsic director force and stress, as follows:

$$t_{ji} = - p\, \delta_{ji} + \hat{t}_{ji} \tag{2.3a}$$

$$g_i = \gamma n_i - \beta_j\, n_{i,j} + \hat{g}_i \tag{2.3b}$$

$$\pi_{ji} = n_i \beta_j + \hat{\pi}_{ji} \tag{2.3c}$$

Here $\hat{t}_{ji}$ is the extra-stress tensor, $\hat{g}_i$ is the intrinsic director extra body force, $\hat{\pi}_{ji}$ is the director extra stress, p is the pressure, and γ is the director tension. The constitutive equations are [1]

$$\hat{t}_{ji} = - \frac{\partial F}{\partial n_{k,j}}\, n_{k,i} + \alpha_1 n_k n_m A_{km}\, n_i n_j + \alpha_2 n_j N_i + \alpha_3 n_i N_j + \alpha_4 A_{ji} \tag{2.4a}$$

$$+ \alpha_5\, n_j n_k A_{ki} + \alpha_6\, n_i n_k A_{kj}$$

$$\hat{g}_i = - \frac{\partial F}{\partial n_i} + \lambda_1 N_i + \lambda_2 A_{ij} n_j \tag{2.4b}$$

$$\hat{\pi}_{ji} = \frac{\partial F}{\partial n_{i,j}} \tag{2.4c}$$

where

$$\lambda_1 = \alpha_2 - \alpha_3 \tag{2.5a}$$

$$\lambda_2 = \alpha_5 - \alpha_6 = - (\alpha_2 + \alpha_3) \tag{2.5b}$$

The $\{\alpha_i\}$, $i = 1,\ldots 6$, are material constants with the dimensions of viscosities. The equality between $\alpha_6 - \alpha_5$ and $\alpha_2 + \alpha_3$ is due to Parodi [17], and is based on arguments from irreversible thermodynamics. The kinematical

quantities appearing in the constitutive equations are defined as follows:

$$N_i = \dot{n}_i - W_{ik} n_k \tag{2.6a}$$

$$\Omega_{ik} = \left(V_{i,k} - V_{k,i}\right)/2 \tag{2.6b}$$

$$A_{ik} = \left(V_{i,k} + V_{k,i}\right)/2 \tag{2.6c}$$

N_i is the angular velocity of the director relative to that of the fluid, Ω_{ik} is the vorticity tensor, and A_{ik} is the rate-of-deformation tensor. The static stress is defined in terms of derivatives of an energy density, F, which is related to the director field as follows [4,5]:

$$2F = K_{11} (\underline{\nabla}\cdot\underline{n})^2 + K_{22} (\underline{n}\cdot\underline{\nabla} \times \underline{n})^2 + K_{33} (\underline{n} \times \underline{\nabla} \times \underline{n})^2 \tag{2.7}$$

The $\{K_{ii}\}$ are elastic constants, referring to splay (11), twist (22), and bend (33) deformations, respectively.

The rheological coefficients $\{\alpha_i\}$ and $\{K_{ii}\}$ can be measured using light scattering and in viscometric flows with external fields (see, for example, deGennes [6]). The most completely studied monomeric nematic liquid crystals are p-azoxyanisole (PAA) and N-(p-methoxybenzylidene)-p'-butylaniline (MBBA). Parameter values for these liquids are tabulated in Table 1. The data for PAA are those used by Tseng et al. [18]; the elastic constants for MBBA are those of de Jeu et al. [19], while the viscosity coefficients are those reported by Gähwiller [20] at 25°C. These are the parameters used in all subsequent calculations.

The remainder of this section is concerned with the detailed development of the reduction of these equations to the form appropriate to Jeffrey-Hamel flow. Jeffrey-Hamel flows are best described in a cylindrical (r, ψ, z) coordinate system; see Figure 1. The radial distance r is measured from the

vertex of the plates. The total enclosed angle between the plates is $2\psi_o$. We assume that the flow is radial, with no variations in the neutral (z) direction, so that $v_z = v_\psi = 0$. Following the classical approach for a Newtonian fluid (see, for example, Denn [21]), we then seek a solution of the form

$$v_r = \frac{u(\psi)}{r} \tag{2.8}$$

with the no-slip condition $u(\pm \psi_o) = 0$. The flow rate per unit width, q, is also a fixed system constant:

$$q = \int_{-\psi_o}^{\psi_o} u(\psi) d\psi \tag{2.9}$$

Note that both u and q are positive for diverging flow and negative for converging flow.

Following Leslie [11], we assume that the director is in the ψ-r plane:

$$n_r = \cos W(\psi) \quad n_\psi = \sin W(\psi) \tag{2.10}$$

The components of the director surface stress tensor and the intrinsic director body force are then as follows:

$$r\pi_{rr} = \cos(W)\ (1+W')\ \left[K_{11} - K_{33} \sin^2(W)\right] \tag{2.11a}$$

$$r\pi_{\psi\psi} = \cos(W)\ (1+W')\left[K_{11} + K_{33}\ \sin^2(W)\right] \tag{2.11b}$$

$$r\pi_{r\psi} = K_{33}\ \sin(W)\ \cos^2(W)\ (1+W') \tag{2.11c}$$

$$r\pi_{\psi r} = -\ K_{33}\sin^3(W)\ (1+W') \tag{2.11d}$$

$$r^2 g_r = -\ \cos(W)\ [1+W']\left[K_{11} + K_{33}\ \sin^2(W)\ \cos(W)\right] + \frac{\lambda_2-\lambda_1}{2}\ \sin(W)\ u' - \lambda_2\ \cos(W)\ \frac{u}{r^2} + \gamma\ \cos(W) \tag{2.12a}$$

$$r^2\ g_\psi = -\ K_{33}\ \sin(W)\left[(W')^2 + \left(1+\sin^2(W)\right) + (W')\left(2+\sin^2(W)\right)\right] + \frac{\lambda_1+\lambda_2}{2}\ \cos(W)\ u' + \lambda_2\ \sin(W)\ u + \gamma\ \sin(W) \tag{2.12b}$$

A prime denotes differentiation with respect to ψ.

The director balance equations (2.2), take the following form for the assumed kinematics:

$$rg_r + (\pi_{rr} - \pi_{\psi\psi}) + \pi_{\psi r,\psi} = 0 \tag{2.13a}$$

$$rg_\psi + (\pi_{\psi r} + \pi_{r\psi}) + \pi_{\psi\psi,\psi} = 0 \tag{2.13b}$$

By combining these balance equations with the preceding stress and body force equations we then obtain a single equation for the director angle, $W(\psi)$:

$$\frac{g'}{2}\ W'(1+W') + gW'' + \left[\lambda_2\ \cos(2W) + \lambda_1\right]\frac{u'}{2} + \left[\lambda_2\ \sin(2W)\right] u = 0 \tag{2.14}$$

Here

$$g(W) = K_{11}\ \cos^2(W) + K_{33}\ \sin^2(W) \tag{2.15a}$$

$$g'(W) = (K_{33} - K_{11})\ \sin\ (2W) \tag{2.15b}$$

This equation simplifies for the commonly-employed approximation of equal elasticity coefficients, $K_{11} = K_{22} = K_{33} = K$, in which case $g(W) = K$ and $g'(W) = 0$. We have not used this simplification in our numerical calculations, although it is used in the asymptotic analysis of the boundary layer.

The components of the stress tensor, Equation (2.4a), are as follows for the assumed kinematics:

$$r^2 \hat{t}_{rr} = R_1 u + R_2 u' \tag{2.16a}$$

$$r^2 \hat{t}_{\psi\psi} = -g - 2gW' - g(W')^2 + R_3 u + R_4 u' \tag{2.16b}$$

$$r^2 \hat{t}_{r\psi} = -\frac{g'[1+(W')]^2}{2} + R_5 u + R_6 u' \tag{2.16c}$$

$$r^2 \hat{t}_{\psi r} = R_7 u + R_8 u' \tag{2.16d}$$

The coefficients $\{R_i\}$, $i = 1$ to 8, are functions of the viscosities $\{\alpha_i\}$ and the director angle $W(\psi)$; these functions are enumerated in Appendix I.

The components of the linear momentum balance equations with the assumed kinematics are as follows:

r-component:

$$-\frac{\rho u^2}{r^3} = t_{rr,r} + \frac{1}{r} t_{\psi r,\psi} + \frac{t_{rr} - t_{\psi\psi}}{r} \tag{2.17a}$$

ψ-component:

$$0 = \frac{t_{r\psi} + t_{\psi r}}{r} + \frac{1}{r} t_{\psi\psi,\psi} + t_{r\psi,r} \tag{2.17b}$$

It should be noted that the stress is asymmetric, so that the order of subscripts on stress terms is important. The isotropic pressure must be of the following form for consistency:

$$p = \frac{\sigma(\psi)}{r^2} \tag{2.18}$$

Combination of Equations (2.16) through (2.18) then leads to the following coupled ordinary differential equations for the scalar functions $u(\psi)$ and $\sigma(\psi)$:

$$g(1 + W')^2 + \rho u^2 + a_1 u + a_2 uW' + a_3 u' + a_4 u'W' + a_5 u'' + 2\sigma = 0 \tag{2.19a}$$

$$\frac{g'}{2} - \frac{3}{2} g'(W')^2 - g'(W')^3 - 2gW'' - 2gW'W'' + a_6 u' + a_7 uW' + a_8 u'W' + a_9 u'' - \sigma' = 0 \tag{2.19b}$$

The coefficients $\{a_i\}$, $i = 1,\ldots 9$, which are tabulated in Appendix I, are functions only of the viscosities and the function $W(\psi)$. Equations (2.14) and (2.19) define the director orientation, the velocity distribution, and the pressure field.

Equations (2.14) and (2.19) are solved here in dimensionless form; the non-dimensionalization and the resulting dimensionless equations and boundary conditions are enumerated in Appendix I. The velocity is scaled with the flow rate per unit width, q, and the elastic terms with the elastic energy coefficient K_{11}; the kinematics are then described by two dimensionless groups, as follows:

$$E = \frac{\lambda_1 q}{K_{ii}} \tag{2.20a}$$

$$R\,E = \frac{\rho q^2}{K_{ii}} \tag{2.20b}$$

E is the *Ericksen number* for this flow, defining the relative overall weights of the viscous and elastic stress terms. K_{11} is chosen as the normalizing elastic coefficient because the dominant deformation with planar boundary conditions is splay (c.f deGennes [6], Chandresekhar [22]); K_{33} could be used when bend deformations dominate, but the two coefficients are of comparable magnitude in any event. The group RE defines the relative

overall weighting of inertial and elastic stress; R is a pseudo-Reynolds number equal to $\rho q/\lambda_1$. R is of order 10^{-4} relative to E for parameters characteristic of monomeric nematic liquid crystals, so the inertial contribution is generally negligible; we have retained the inertial term in our numerical calculations for generality, but the effect is never significant.

All calculations of the boundary value problem reported subsequently were obtained using the Galerkin finite element technique with quadratic shape functions over thirty spatial elements (e.g., Fletcher [23]). Newton-Raphson iteration was used for solution of the nonlinear system of algebraic equations. Convergence was very sensitive in many cases to the selection of the initial estimate, and first-order continuation in the material properties and the director wall orientation was generally necessary.

III. Centerline Orientation

Symmetry of the velocity profile and antisymmetry of the director orientation are assumed to exist around the centerline, $\psi = 0$. There are multiple solutions to the equation set, and two possible director orientation distributions can exist; these are characterized by aligned ($W = 0$) and transverse ($W = \pm\pi/2$) orientations at the centerline. Convergence to the correct solution can be ensured by using only the half space $0 \le \psi \le \psi_o$ and setting the centerline boundary condition, rather than using symmetry. The boundary condition can be determined by a linear stability analysis.

We denote the steady-state director as $W_s(\psi)$, and we perturb the director field about $W_s(\psi)$ while retaining the steady-state velocity distribution. The orientation is now given by

$$W(\psi,r,t) = W_s(\psi) + W_d(\psi,r,t) \tag{3.1}$$

Neglecting elastic torques, which will be negligible along the centerline at sufficiently high values of the Ericksen number, the time-dependent director

equation is then

$$\lambda_1 r^2 \frac{\partial W_d}{\partial t} + \left[\lambda_2 \cos (2W) + \lambda_1\right] \frac{u'}{2} + \left[\lambda_2 \sin (2W)\right] u = 0 \qquad (3.2)$$

and, expanding the sine and cosine about the steady solution and retaining only first-order terms in the perturbation, we obtain

$$\lambda_1 r^2 \frac{\partial W_d}{\partial t} + \left[-2\lambda_2 W_d \sin (2W_s)\right] \frac{u'}{2} + \left[2\lambda_2 \cos(2W_s) W_d\right] u = 0 \qquad (3.3)$$

$u' = 0$ at the centerline; defining $\lambda = \lambda_2/\lambda_1$ we thus obtain

$$\frac{\partial W_d(0)}{\partial t} = -\left\{\frac{2\lambda}{r^2} \cos(2W_s(0))\, u(0)\right\} W_d(0) \qquad (3.4)$$

λ is negative and greater in absolute value than unity for the physical parameters considered here; this corresponds to the case of no "tumbling" of the director. $u(0)$ is negative for inflow (converging flow) and positive for outflow (diverging flow), so the stable solution for converging flow corresponds to $W_s(0) = 0$ (alignment) and for diverging flow to $W_s(0) = \pm\pi/2$ (transverse). We shall show subsequently that this boundary condition can be changed by introduction of additional centerline torques on the director through imposition of an electromagnetic field.

IV. Similarity Solutions

The normalized velocity profile in a converging channel with $\psi_o = 0.5$ is shown as curve A in Fig. 2 for the parameters characteristic of PAA and a wall anchoring angle for the director of $\pi/6$. Curve B is the profile for the same material parameters, but with the elastic coefficients $\{K_{ii}\}$ set to zero the wall anchoring angle is now fixed by the material parameters. Curve C is the profile for a Newtonian fluid; the creeping-flow profile for

the Newtonian fluid is (see, e.g., Denn, [21]).

$$u(\psi) = \left[\frac{\cos 2\psi - \cos 2\psi_o}{\sin 2\psi_o - 2\psi_o \cos 2\psi}\right] q \qquad (4.1)$$

Elasticity has no effect on this scale on the velocity profile. The profiles for PAA and a Newtonian fluid are also very close for the given flow rate and anchoring angle. This invariance of the velocity profile will be exploited subsequently in some closed-form analytical approximations.

The orientation of the director as a function of angular position is plotted for various anchoring angles in Fig. 3. There is some arbitrariness about the quantity to be kept constant in such comparisons; we have selected the wall isotropic pressure (which is equivalent to selecting the total reference pressure at a point far upstream) as the constant throughout this work whenever the point to be illustrated involves changing a physical parameter or a boundary condition, in which case the flow rate may vary. It can be seen in Fig. 3 that there are two distinct regions in the flow: There is a core region, in which the orientation of the director is determined solely by the flow effects of shear and elongation; the elastic torques are negligible in this region, and the viscous torques must sum to zero. There is a boundary layer region close to the wall, in which the elasticity of the fluid propagates the fixed orientation at the wall.

The effect of elasticity is shown in Fig. 4, where the viscosities for PAA are used and the wall anchoring angle is again taken to be $\pi/6$. The boundary layer thickness decreases with decreasing values of the elastic constants (K_{ii}). The limit of vanishing elastic constants, which corresponds to Ericksen's TIL, is singular; the wall condition is forced to be the solution to $\cos 2W(\psi_o) = -1/\lambda$, and no condition imposed by the physics of

interaction between the nematic liquid and the wall can be satisfied. This observation is undoubtedly important with regard to analyses applying the TIL constitutive equation to liquid crystalline polymers, since the wall orientation angle for rigid polymers is expected to be zero.

The effect of varying the Ericksen number (by changing the reference pressure) is illustrated in Figs. 5a and b; the anchoring angle is $\pi/6$ in the former and zero in the latter. The elasticity boundary layer is clearly seen here. The thickness of the boundary layer is a decreasing function of E.

The director orientation angle at two angular positions is shown as a function of Ericksen number in Fig. 6 for the two nematic liquids considered here. The core solution is achieved rapidly in curves C and D, which are for a position close to the center line; the core has not yet been achieved at a position within 0.25 radians of the wall for $E > 3000$. The rather similar behavior of the two liquids is a consequence of the non-dimensional formulation of the problem.

Velocity profiles for diverging flow of a fluid with the properties of PAA are shown in Fig. 7. Curve A is for the L-E fluid with a wall angle of zero, while for curve B the wall angle for this case is $-\pi/6$ radians. Curve C is for a Newtonian liquid. The velocity profiles are still quite close, but the difference between the nematic and Newtonian profiles is somewhat greater here than for the converging flow computed in Fig. 2.

The effect of the anchoring angle on the orientation profile in diverging flow is shown in Fig. 8. The boundary layer induced by the elasticity and the wall alignment is clearly seen. Because of the stable transverse orientation at the centerline, the core solution for diverging flow is not close to alignment with the flow; rather, there is a gradual

transition involving large rotations from the transverse orientation in the bi-axially-expanding centerline region to the near-alignment in the shear-dominated wall region.

V. Significance of the Asymmetric (Elastic) Stresses

It is of some interest to compare the flow behavior of the Leslie-Ericksen nematic liquid with Ericksen's Transversely Isotropic Liquid, to which the former reduces in the limit of vanishing elasticity constants. As we have already noted, this limit is singular. This comparison is motivated in part by the claim of Vanderheyden and Ryskin [12] that, because the elastic stresses in a polymer liquid crystal are small relative to the viscous stresses, the elastic constants may be set to zero in a flow analysis.

Leslie's [1] constitutive equation (2.4a) for the asymmetric stress tensor of a nematic liquid crystal can be resolved into symmetric and antisymmetric components, as follows:

$$\hat{t}_{ij} = \tilde{t}_{ij}^{\,s} + \tilde{t}_{ij}^{\,a} - \frac{\partial F}{\partial n_{k,i}} n_{k,j} \tag{5.1}$$

$$\begin{aligned}\tilde{t}_{ij}^{\,s} = {} & \alpha_1 A_{kp} n_k n_p n_i n_j + \alpha_4 A_{ij} + \frac{1}{2}(\alpha_2+\alpha_3)(n_i N_j + N_i n_j) \\ & + \frac{1}{2}(\alpha_5+\alpha_6)(A_{ki} n_k n_j + A_{kj} n_k n_i)\end{aligned} \tag{5.2a}$$

$$\tilde{t}_{ij}^{\,a} = \frac{1}{2}(\alpha_2-\alpha_3)(N_j n_i - n_j N_i) + \frac{1}{2}(\alpha_5-\alpha_6)(A_{ki} n_j n_k - A_{kj} n_i n_k) \tag{5.2b}$$

Since the antisymmetric stresses couple the velocity and director fields

through the action of viscous torques, a symmetric stress tensor without elastic terms will result in an orientation field of vanishing viscous torques; in our case this is given by Eqn. (2.14) with $g = g' = 0$, as follows:

$$[\lambda \cos(2W) + 1] \frac{u'}{2} + [\lambda \sin(2W)] u = 0 \qquad (5.3)$$

where $\lambda = \lambda_2/\lambda_1$. Equation (5.3) is identical to Leslie's [11] director equation for an anisotropic fluid with no elasticity, and hence with a symmetric stress tensor. For the same value of the physical constant λ the core solutions for the two fluids will be the same, but the elastic L-E liquid will deviate from this solution to achieve the specified anchoring angle. To achieve the same wall orientation, the inelastic TIL would require a different value of λ, and the orientation profile would therefore be drastically different; i.e., the wall anchoring boundary condition cannot be satisfied without changing the properties of the fluid, and hence the orientation distribution throughout the bulk. It is therefore clear that, to the extent that the L-E theory might approximate the behavior of polymer liquid crystals, the elastic stresses must be retained in any flow analysis if the orientation distribution is to be computed. Thin orientation boundary layers are expected because of the tendency of the rod-like macromolecules to align with the surface of a die. This boundary layer would lie between the wall and any orientation induced near the wall by the bulk flow.

VI. Boundary Layer Analysis

Boundary layer behavior of nematic liquid crystals in shear flows is described in the review by Leslie [8] and the book by de Gennes [6]. More recently, Skarp and Carlsson [25] studied the orientation boundary layer in

shear flow in the presence of electric fields. We carry out a similar analysis for Jeffrey-Hamel flows without external fields in this section, and we obtain an approximate analytical expression for the boundary layer thickness as a function of the Ericksen number.

Equation (5.3) describes the orientation distribution in the core region, where there are no elastic torques; the solution is

$$\tan W_c = \frac{-2\lambda u \pm \sqrt{4\lambda^2 u^2 - \left(1-\lambda^2\right)(u')^2}}{u'(1-\lambda)} \tag{6.1}$$

where $\lambda = \lambda_2/\lambda_1$ and the subscript "c" refers to the core. The negative sign applies for inflow and the positive sign for outflow.

We seek a solution valid near the wall in the form of a perturbation about the core solution, as follows:

$$W = W_c + \epsilon W_i \tag{6.2}$$

ϵ is a small parameter. The "inner" solution, W_i, is required in order to satisfy the wall orientation boundary condition. By assuming the one constant approximation ($K_{11} = K_{22} = K_{33} = K$) we then obtain (see Appendix II) the following equation for W_i:

$$W_i'' - \lambda\left[\sin\left(2W_c\right)\right]EU'W_i + 2\lambda\left[\cos\left(2W_c\right)\right]EU\,W_i = 0 \tag{6.3}$$

It is convenient to measure the angle from the wall, and we define $\phi = \psi_o - \psi$. We assume that the velocity profile is approximately linear in the wall region,

$$U = \beta\phi \tag{6.4}$$

where β is known in closed form for Newtonian fluids in the creeping flow limit (Eq. 4.1) We further assume that W_c in the neighborhood of the wall is fixed at the "natural" wall value given by $\cos 2W_c = -1/\lambda$ (see Appendix II); this is a reasonable approximation for converging flow, but it is likely to be innacurate for diverging flow (c.f. Fig. 8). These assumptions result in the following linear equation for the inner solution:

$$W_i'' - \left[2E\beta(\mu+\phi)\right] W_i = 0 \tag{6.5}$$

where

$$\mu = \frac{\sqrt{\lambda^2-1}}{2} \tag{6.6}$$

Equation (6.5) is singular in the limit $E \to \infty$, for which special care must be taken. The solution is given in terms of Airy functions, as follows:

$$W_i = C_1 A_i(z) + C_2 B_i(z) \tag{6.7}$$

Here $z = (2E\beta)^{1/3}(\mu + \phi)$ and A_i and B_i are Airy functions of the first and second kind, respectively. B_i is unbounded, so the condition that W_i be bounded for large ϕ requires that $C_2 = 0$. We thus obtain the following solution:

$$W_i(\psi) = \frac{W_{i,w}}{A_i\left(E^{1/3}(2\beta)^{1/3}\mu\right)} A_i\left(E^{1/3}(2\beta)^{1/3}(\mu+\phi)\right) \tag{6.8}$$

The Airy function of the first kind goes asymptotically to zero as the argument becomes large. The boundary layer thickness is thus estimated by

$$\delta(E) = \frac{2}{E^{1/3}\,(2\beta)^{1/3}} - \frac{(\lambda^2-1)^{1/2}}{2} \tag{6.9}$$

where we have defined δ as that distance for which $A_i(E^{1/3}(2\beta)^{1/3}(\mu+\delta))$ is sufficiently close to zero, say 0.03.

In order to avoid the singularity in the limit $E \to \infty$, the problem must be rescaled. We define a new angle,

$$\xi = \phi E^n \tag{6.10}$$

where the exponent n is to be determined. Equation (6.5) then becomes

$$E^{2n}\,\frac{d^2W_i}{d\xi^2} - 2E\beta\left(\mu + \xi E^{-n}\right) W_i = 0 \tag{6.11}$$

n must equal 1/2 in order for the equation to remain regular as $E \to \infty$. In this limit the equation becomes identical to that for simple shear, with a boundary layer thickness of [24]

$$\delta(E) = \frac{3.5}{(E\beta)^{1/2}(\lambda^2 - 1)^{1/4}} \tag{6.12}$$

The constant 3.5 appears so that there is consistency with the previous boundary layer definition given by Eq. (6.9). The square root dependance can also be obtained from an asymptotic solution to Eq. (6.5) using the WKB approximation (see e.g., Nayfeh [26]).

The approximation that W_c can be approximated by the wall value throughout the boundary layer is too crude for outflow, where W_c varies

uniformly from the the "natural" value at the wall (typically close to zero) to $\pm\pi/2$ at the centerline; see Appendix II. The limiting behavior for $E \to -\infty$ is unchanged, except that E must be replaced by $|E|$ in Eq. (6.12). The differential equation now contains a turning point, however, and the cube-root behavior is not recovered; the turning point occurs near the transition in the boundary-layer behavior, and reflects the different core solution for outflow.

Figure 9 shows a plot of the boundary layer thickness as a function of Ericksen number. The continuous curve labeled "numerical solution" was obtained by estimating the boundary layer thickness from curves like those in Figs. 5 and 8. Agreement with the asymptotic solutions given by Eqs. (6.9) and (6.12) is excellent for inflow, and agreement with the solution given by Eq. (6.12 is excellent for outflow. The boundary layer thickness is determined for inflow by the competition between wall alignment and the extensional flow in the core for E below 2000, leading to the $-1/3$ dependence. At higher Ericksen numbers the boundary layer is sufficiently thin that the flow in the core has little significance, and the competition is between the wall anchoring and the shear flow near the wall. In this case the boundary layer is determined in the same manner as in a shear flow, and the $-1/2$ power dependence characteristic of shear flows is recovered for both inflow and outflow.

VII. Magnetohydrodynamics

Liquid crystalline molecules are diamagnetic, and macroscopic orientation can be effected through the use of electro-magnetic fields; see Moore and Denn [16], for example, for a discussion of magnetically-induced orientation in liquid crystalline polymers. The use of external fields with

flow could have processing significance as a means of controlling orientation distributions. In this section we obtain and discuss solutions to converging and diverging flows in which there are imposed magnetic fields.

As shown by Ericksen [27,28], a magnetic field affects the fluid through the action of a body force $\underline{F}$ and a body couple $\underline{n} \times \underline{G}$, as follows:

$$\underline{F} = \left[\left(\chi_\perp \underline{H} + \Delta\chi(\underline{n}\cdot\underline{H})\underline{n}\right)\cdot\nabla\right] \underline{H}$$
$$\underline{n}\times\underline{G} = \underline{n} \times [\Delta\chi(\underline{n}\cdot\underline{H})] \underline{H} \tag{7.1}$$

$\chi_\perp$ and $\chi_{||}$ are the magnetic susceptibilities perpendicular and parallel to the director, respectively, and $\Delta\chi = \chi_\perp - \chi_{||}$ is the anisotropic magnetic susceptibility. Compatability with the similarity solution and the Maxwell equations requires that the magnetic field have the following form:

$$\underline{H} = \left(\frac{A}{r}, \frac{B}{r}, 0\right) \tag{7.2}$$

The extrinsic director body force $\underline{G}$ and the external body force $\underline{F}$ then have the following components:

$$G_r = \Delta\chi \frac{A}{r^2} [A.\cos(W) + B \sin(W)] \tag{7.3a}$$

$$G_\psi = \Delta\chi \frac{B}{r^2} [A \cos(W) + B \sin(W)] \tag{7.3b}$$

$$F_r = -\frac{\chi_\perp}{r^3}\left(A^2+B^2\right) - \frac{\Delta\chi}{r^3}\left(A^2\cos^2(W) + B^2 \sin^2(W) + AB \sin(2W)\right)$$
$$F_\psi = \frac{\Delta\chi}{r^3}\left[-AB \cos(2W) + \left(A^2 - B^2\right) \sin(W) \cos(W)\right] \tag{7.4}$$

The dimensionless form of the balance equations (see Appendix I) leads to an additional dimensionless group, known as the *Zocher number*, Z:

$$Z^2 = \frac{\left(A^2+B^2\right)\Delta\chi}{K_{11}} \tag{7.5}$$

The Zocher number gives the relative magnitude of magnetic to elastic torques; the relative magnitude of viscous to magnetic torques is given by

$$D = \frac{E}{Z^2} = \frac{\lambda_1 q}{\left(A^2+B^2\right)\Delta\chi} \tag{7.6}$$

Values of the magnetic susceptibilities from Gasparoux et al. [29] are included in Table 1. Numerical computations of the orientation profile in converging flow with a radial magnetic field are shown in Fig. 10. The magnetic field influences the flow in two ways: the field induces director alignment in the radial direction, thus acting cooperatively with the flow-induced alignment; the field also causes a position-dependent body force. The latter causes an effective pressure gradient that acts against the flow, and hence retards the motion and reduces the Ericksen number for a fixed wall reference pressure. A field of sufficient strength can cause the flow to reverse direction.

The effect of an azimuthal field on a converging flow is expected to be qualitatively different. The magnetic body force still acts to retard the flow, with flow reversal possible for a sufficiently strong field, but the field tends to induce a transverse alignment during inflow. There is therefore a competition between the field and the flow, and the retarding effect of the magnetic body force gradient at a constant wall reference pressure enhances the aligning strength of the field. Computed orientation distributions for increasing azimuthal field strengths in converging flow

are shown in Figure 11, illustrating the increasing tendency towards transverse alignment. The director equations admit multiple solutions, with both aligned and transverse orientations possible at the centerline. It might be expected that for a sufficiently strong transverse field there would be an exchange of stability in a converging flow at a critical field strength to the transverse centerline orientation.

Including the magnetic field in the balance equations results in the additional term + $\Delta\chi B^2 \cos(2W_s(0))/\lambda_1 r^2$ in the braces on the right-hand side of Eq. (3.4); the condition for stability of the radial orientation then includes both flow and field-strength terms, as follows:

$$2\lambda_2 u(0) + \Delta\chi B^2 \; < \; 0 \tag{7.6}$$

There is a critical field given by

$$B_c = \sqrt{\frac{-2\lambda_2 u(0)}{\Delta\chi}} \tag{7.7a}$$

or, in dimensionless form,

$$D_c = -\frac{1}{2\lambda U(0)} \tag{7.7b}$$

The group $-2\lambda U(0)$ is plotted versus $1/D$ in Figure 12 for the family of converging flow solutions with an aligned centerline orientation; this plot includes the solutions shown in Figure 11. Flow reversal occurs as $D \rightarrow 0$ (c.f. Eq. 7.5), or $1/D \rightarrow \infty$. The critical condition for transition corresponds to the intersection of the curve of $-2\lambda U(0)$ with the 45° line,

which occurs at D close to .47, and thus considerably before flow reversal; use of the Newtonian velocity profile in Eq. (7.7) gives a critical value of $D_c \sim 0.59$.

These results establish the existence of a new first-order transition in flow that is analogous to the Freedericksz transition in quiescent liquid crystals [6], except that the latter is second-order. In the Freedericksz transition the field overcomes the alignment induced by the wall, and the balance is between magnetic and elastic torques; in the flow transition, the magnetic field overcomes the aligning torque induced by the extensional flow. The transverse orientation will remain stable as the field strength is increased, since the flow will become progressively weaker and eventially reverse. Orientation distributions just before and after the transition are shown in Figure 13, together with the orientation at reversal to outflow.

The azimuthal magnetic field can be realized by use of a current-carrying wire at the vertex of a converging flow, and the transition will be easily-observable by a change in the transmision intensity of polarized light. The grouping of viscosities given by λ_2 (Eq. 2.5b) can then be determined by measuring the critical field strength and flow rate for a given wall reference pressure; the centerline velocity can be estimated with sufficient accuracy by using the Newtonian fluid centerline velocity.

There is no transition with outflow. A radial field increases shear, hence aligning the director closer to the radial direction, but the centerline compression stabilizes the transverse orientation. The stability criterion is always satisfied, leading to a sharp "wall-like" profile near the centerline; c.f. Fig. 14. An azimuthal field in the diverging flow will stabilize the center line orientation both through the added viscous torques and the magnetic torques.

Acknowledgment

This work was supported in part by the Donors of the Petroleum Research Fund (ADR) and in part by the Director, Office of Energy Research, Office of Basic Energy Sciences, Materials Science Divison of the U. S. Department of Energy under Contract No. DE-AC03-76SF00098 (MMD).

Appendix I

The coefficients $\{R_i\}$ in Equations (2.15) are as follows:

$$R_1 = -\alpha_1 \cos(2W) \cos^2(W) - \alpha_4 - (\alpha_5 + \alpha_6) \cos^2(W) \tag{I.1a}$$

$$R_2 = \alpha_1 \cos(W) \cos^3(W) + \alpha_5 \sin(W) \cos(W) \tag{I.1b}$$

$$R_3 = -\alpha_1 \sin^2(W) \cos(2W) + \alpha_4 + (\alpha_s + \alpha_6) \sin^2(W) \tag{I.1c}$$

$$R_4 = \alpha_1 \sin^3(W) \cos(W) + \frac{\left(\alpha_5+\alpha_6\right)}{2} \sin(W) \cos(W) + \left(\frac{\alpha_2+\alpha_3}{2}\right) \sin(W) \cos(W) \tag{I.1d}$$

$$R_5 = -\frac{\alpha_1}{4} \sin(4W) + \left(\frac{\alpha_5-\alpha_6}{2}\right) \sin(2W) \tag{I.1e}$$

$$R_6 = \alpha_1 \sin^2(W) \cos^2(W) + \frac{\alpha_2}{2} \cos^2(W) - \frac{\alpha_3}{2} \sin^2(W) + \frac{\alpha_4}{2} + \frac{\alpha_5}{2} \cos^2(W) + \frac{\alpha_6}{2} \sin^2(W) \tag{I.1f}$$

$$R_7 = -\frac{\alpha_1}{4}\sin(4W) - \frac{(\alpha_5-\alpha_6)}{2}\sin(2W) \qquad \text{(I.1g)}$$

$$R_8 = \alpha_1 \sin^2(W)\cos^2(W) - \frac{\alpha_2}{2}\sin^2(W) + \frac{\alpha_3}{2}\cos^2(W) + \frac{\alpha_4}{2} + \frac{\alpha_5}{2}\sin^2(W) + \frac{\alpha_6}{2}\cos^2(W) \qquad \text{(I.1h)}$$

The coefficients $\{a_i\}$ in Equations (2.19) are as follows:

$$a_1 = \alpha_1 \cos2W + (\alpha_5+\alpha_6)\cos2W \qquad \text{(I.2a)}$$

$$a_2 = -\alpha_1 \cos4W - (\alpha_5-\alpha_6)\cos2W \qquad \text{(I.2b)}$$

$$a_3 = -\alpha_1 \cos^2W \sin2W - \alpha_5 \sin2W \qquad \text{(I.2c)}$$

$$a_4 = \frac{\alpha_1}{2}\sin2W + (\alpha_5-\alpha_6)\sin2W \qquad \text{(I.2d)}$$

$$a_5 = \frac{\alpha_1}{2} \sin 2W + \left(\frac{\alpha_5 - \alpha_6}{2}\right) \sin^2 W + \left(\frac{\alpha_3 + \alpha_6}{2}\right) \cos^2 W \qquad \text{(I.2e)}$$

$$a_6 = -\alpha_1 \sin^2 W \cos 2W + \alpha_4 + (\alpha_5 + \alpha_6) \sin^2 W \qquad \text{(I.2f)}$$

$$a_7 = \alpha_1 (1 - 2\cos W) \sin 2W + (\alpha_5 + \alpha_6) \sin 2W \qquad \text{(I.2g)}$$

$$a_8 = \frac{\alpha_1}{2} (\cos 2W - \cos 4W) + \alpha_6 \cos 2W \qquad \text{(I.2h)}$$

$$a_9 = \alpha_1 \sin^3 W \cos W + \alpha_6 \sin W \cos W \qquad \text{(I.2i)}$$

The Parodi relation, Eq. (2.5b), has been used to simplify some equations.

The nondimensional equations are obtained by scaling the velocity with q, the elastic terms and the angular dependence of pressure with K_{11}, and the viscosity coefficient terms with λ_1. The following dimensionless groups result:

$$Y = \frac{g}{K_{11}} \qquad \Sigma = \frac{\sigma}{K_{11}}$$

$$U = \frac{u}{q} \qquad E = \frac{\lambda_1 q}{K_{11}}$$

$$A_i = \frac{a_i}{\lambda_1} \qquad RE = \frac{\rho q^2}{K_{11}}$$

$$\lambda = \frac{\lambda_2}{\lambda_1}$$

Equations (2.14) and (2.19) then become the following fifth-order set of nondimensional nonlinear ordinary differential equations:

$$RE \frac{U^2}{Y} + (1 + W')^2 + A_1 E \frac{U}{Y} + A_2 E \frac{UW'}{Y} + A_3 \frac{EU'}{Y} + A_4 E \frac{U'W'}{Y} + A_5 E \frac{U''}{Y} + 2\frac{\Sigma}{Y} = 0 \qquad \text{(I.3a)}$$

$$\frac{1}{2} - \frac{3}{2} W'^2 - W'^3 - \frac{G}{Y'} W'' - \frac{2G}{Y'} W'W'' + A_6 E \frac{U'}{Y'} + A_7 \frac{EW'}{Y'} + A_8 E \frac{U'W'}{Y'} + A_9 EU'' - \frac{\sum'}{Y'} = 0 \tag{I.3b}$$

$$W'' + \frac{Y'}{2Y} W' + \frac{Y'}{2Y} W'^2 + \left(\frac{\lambda}{2} \cos 2W + \frac{1}{2}\right) \frac{EU'}{Y} + (\lambda \sin 2W) \frac{EU}{Y} = 0 \tag{I.3c}$$

The boundary conditions are as follows:

$$U\left(\pm\psi_o\right) = 0 \qquad \text{No slip at the wall} \tag{I.4a}$$

$$\sum\left(\pm\psi_o\right) = \sum_o \qquad \text{Fixed reference pressure at the wall} \tag{I.4b}$$

$$W\left(\pm\psi_o\right) = W_o \qquad \text{Fixed anchoring angle at the wall} \tag{I.4c}$$

The director external body force takes on the following form when there is an imposed magnetic field, $\underline{H}$:

$$\underline{G} = \Delta\chi \, (\underline{n} \cdot \underline{H}) \, \underline{H} \tag{I.5}$$

The director balance equations thus become

$$\frac{g'W'}{2} (1+W') + gW'' + \left(\lambda_2 \cos 2W + \lambda_1\right) \frac{u'}{2} + (\lambda_2 \sin 2W)u + \Delta\chi \left[\left(B^2 - A^2\right) \sin\phi \cos\phi + AB \cos 2W\right] = 0 \tag{I.6a}$$

or, in dimensionless form,

$$W'' + \frac{Y'}{2Y} W' + \frac{Y'}{2Y} W'^2 + \left(\frac{\lambda \cos 2W}{2} + \frac{1}{2}\right) \frac{EU'}{Y} + (\lambda \sin 2W) \frac{EU}{Y}^2 \tag{I.6b}$$

$$+ \frac{Z^2}{Y} \left[\left[- \frac{A^2-B^2}{A^2+B^2} \right] \frac{\sin 2W}{2} + \left[\frac{AB}{A^2+B^2} \right] \cos 2W \right] = 0$$

The extrinsic body forces are

$$\underline{F} = \left[\left(\chi_{\perp} \underline{H} + \Delta\chi (\underline{n} \cdot \underline{H}) \underline{n} \right) \cdot \underline{\nabla} \right] \underline{H} \qquad \text{(I.7)}$$

The dimensionless momentum balance equations (I.3a) and (I.3b) will then contain the the following additional terms, respectively:

$$- \frac{Z^2}{Y} \left[\frac{\chi_2}{\Delta\chi} + \left[\frac{B^2}{A^2+B^2} \right] + \left[\frac{A^2-B^2}{A^2+B^2} \right] \cos^2(W) + \left[\frac{AB}{A^2+B^2} \right] \sin(2W) \right] \qquad \text{(I.8a)}$$

and

$$\frac{Z^2}{Y'} \left[\left[- \frac{AB}{A^2+B^2} \right] \cos(2W) + \left[\frac{A^2-B^2}{A^2+B^2} \right] \frac{\sin 2W}{2} \right] \qquad \text{(I.8b)}$$

Appendix II

For sufficiently large flow rates the orientation profile consists of a core and wall region. We assume that the boundary layer is a perturbation about the core solution that scales with a small parameter, ϵ:

$$W(\psi) = W_c(\psi) + \epsilon W_i \tag{II.1}$$

The first-order expansions of the trigonometric functions are

$$\cos 2W = \cos 2W_c - 2\,\epsilon\, W_i \sin 2W_c$$
$$\sin 2W = \sin 2W_c + 2\epsilon\, W_i \cos 2W_c$$

With the one-constant approximation for the elastic coefficients, Eq. (2.14) then becomes

$$K\left[W_c'' + \epsilon W_i''\right] + \left[\lambda_2\left(\cos 2W_c - 2\epsilon W_i \sin 2W_c\right) + \lambda_1\right]\frac{u'}{2} + \lambda_2\left[\sin 2W_c + 2\epsilon W_i \cos 2W_c\right] u = 0 \tag{II.2}$$

We then collect terms of equal order in ϵ:

$$O(\epsilon^0): \; KW_c'' + \left[\lambda_2(\cos 2W_c) + \lambda_1\right]\frac{u'}{2} + \lambda_2\left[\sin 2W_c\right] u = 0 \tag{II.3a}$$

$$O(\epsilon^1): \; KW_i'' + \left[\lambda_2\,(-2W_i \sin 2W_c)\right]\frac{u'}{2} + \left[2\lambda_2 W_i \cos 2W_c\right] u = 0 \tag{II.3b}$$

The dimensionless form of Eq. (A2.3) is

$$\frac{W_i''}{W_i} - \lambda EU' \sin(2W_c) + 2\lambda EU \cos 2W_c = 0 \qquad \text{(II.3c)}$$

It is assumed that the flow is sufficiently strong that elastic torques are negligible in the core, in which case we may simplify Eq. (II.3a) by taking $K \to 0$ to obtain an outer solution:

$$KW_c'' = 0: \quad \left[\lambda_2(\cos 2W_c) + \lambda_1\right] \frac{u'}{2} + \left[\lambda_2 \sin 2W_c\right] u = 0 \qquad \text{(II.4)}$$

Using the following trigonometric identities in Eq. (II.4),

$$\cos 2\alpha = \frac{1 - \tan^2\alpha}{1 + \tan^2\alpha}$$

$$\sin 2\alpha = \frac{2 \tan \alpha}{1 + \tan^2\alpha}$$

we obtain the analytical equation for the core orientation, W_c:

$$\tan W_c = \frac{-2\lambda u \pm \sqrt{4\lambda^2 u^2 - \left[1-\lambda^2\right](u')^2}}{u'(1 - \lambda)} \qquad \text{(II.5)}$$

$u(\psi)$ is zero at the wall; we thus obtain the core solution extrapolated to the wall, $W_{c,w}$, as follows:

$$\tan W_{c,w} = \pm \sqrt{\frac{\lambda + 1}{\lambda - 1}} \qquad \text{(II.6a)}$$

For inflow,

$$\cos 2W_{c,w} = -\frac{1}{\lambda} \quad , \quad \sin 2W_{c,w} = -\frac{1}{\lambda}\sqrt{\lambda^2-1} \tag{II.6b,c}$$

It suffices to approximate W_c in Eq. (2.5) by the value at the wall, $W_{c,w}$, in which case we obtain

$$W_i'' + \left[\sqrt{\lambda^2-1}\ EU' - 2EU\right] W_i = 0 \tag{II.7}$$

We further approximate the velocity profile near the wall by the linear approximation to the Newtonian profile in Eq. (4.1), $U = \beta\phi$, where $\beta = -1/(2\alpha - \tan 2\alpha)$ and α is the half angle between the plates. We therefore obtain

$$W_i'' - \left\{2E\beta\left[\frac{\sqrt{(\lambda^2-1)}}{2} + \phi\right]\right\} W_i = 0 \tag{II.8}$$

Bibliography

1. F.M. Leslie, Arch. Rat. Mech. Anal., 28, 265 (1968a).
2. F.M. Leslie, Proc. R. Soc. London, Ser. A., 307, 359 (1968b).
3. J.L. Ericksen, Trans. Soc. Rheol., 5, 23 (1961).
4. C.W. Oseen, Ark. Mat. Astron. Fys., 19A, 1 (1925).
5. F.C. Frank, Discuss. Faraday Soc., 25, 19 (1958).
6. P.G. de Gennes, The Physics of Liquid Crystals, Oxford U. Press, 1975.
7. J.L. Ericksen, in R. Rivlin, ed., The Mechanics of Viscoelastic Fluids, AMD-vol. 22, ASME, 1977.
8. F.M. Leslie, Adv. Liq. Cryst., 4, 1 (1979).
9. J.T. Jenkins, Ann. Rev. Fluid Mech., 10, 197 (1978).
10. T. Carlsson, Ph.D. Dissertation, Institute of Theoretical Physics, Göteborg, 1984.
11. F.M. Leslie, J. Fluid Mechanics, 18, 595 (1964).
12. W.B. Vanderheyden and G. Ryskim, J. Non-Newtonian Fluid Mech., 23, 383 (1987).
13. J.G. Evans, in J.F. Hutton, J.R.A. Pearson, and K. Walters, eds., Theoretical Rheology, London: Applied Science Publ., 1972.
14. G.G. Lipscomb, M.M. Denn, D. Hur, and D.V. Boger, submitted to J. Non-Newtonian Fluid Mech.
15. M. Doi and S.F. Edwards, The Theory of Polymer Dynamics, Clarendon Press, Oxford, 1986.
16. R.G. Moore and M.M. Denn, in A. Zachariades and R. Porter, eds., The Path to High Modulus Polymers with Stiff and Flexible Chains, New York: Marcel Dekker, in press.
17. O. Parodi, J. de Physique, 31, 581 (1970).

18. H.C. Tseng, D.L. Silver, A.B. Finlayson, Phys. Fluids, 15, 1213 (1972).

19. W.H. de Jeu, W.A.P. Claasen, and A.M.J. Sprujit, Mol. Cryst. Liq. Cryst., 37, 263 (1976).

20. Ch. Gähwiller, Mol. Cryst. Liq. Cryst., 20, 301 (1973)

21. M.M. Denn, Process Fluid Mechanics, Prentice-Hall, Inc., Englewood Cliffs, NJ, 1980.

22. S. Chandrasekhar, Liquid Crystals, Cambridge University Press, 1977.

23. C.A.J. Fletcher, Computational Galerkin Methods, Springer Verlag, New York, 1984.

24. J.L. Ericksen, Trans. Soc. Rheol., 13, 9 (1969).

25. K. Skarp and T. Carlsson, Mol. Cryst. Liq. Cryst., 49, 75 (1978).

26. A.H. Nayfeh, Perturbation Methods, John Wiley & Sons, New York, 1973.

27. J.L. Ericksen, Arch. Rational Mech. Anal., 9. 371 (1962).

28. J.L. Ericksen, Arch. Rational Mech. Anal., 23, 266 (1966).

29. H. Gasparoux and J. Proust, J. Phys. (Paris), 32, 953 (1971).

Table I. Physical Constants

Viscosities (poise)	PAA	MBBA
α_1	0.043	0.065
α_2	-0.069	-0.96
α_3	-0.002	-0.011
α_4	0.068	0.832
α_5	0.047	0.63
α_6	-0.023	-0.34
λ_1	-0.067	-0.949
λ_2	0.0705	0.97
Elastic Constants (dynes) x 10^7		
K_{11}	4.9	7.1
K_{33}	10.5	9.2
Diamagnetic Susceptibilities (cgs emu g^{-1}) x10^7		
$\Delta\chi$	1.26	–
$\chi_\perp$	-4.8	–

Figure Captions

Fig. 1. Schematic of Jeffrey-Hamel flow. $W(\psi)$ is the angle of the director with respect to a ray at angle ψ from the centerline. $\psi_o = 0.5$ in all calculations shown here.

Fig. 2. Scaled velocity profile for converging flow, $q = -0.0063$ $cm^2 s$. A: PAA, with $W(\psi_o) = \pi/6$; B: PAA viscosities, but all $K_{ii} = 0$, $W(\psi_o) = 0.158$; C: Newtonian.

Fig. 3. Director orientation profiles for converging flow of PAA, $p(\psi_o, X) = 0.01$ d/cm^2. A: $W(\psi_o) = \pi/3$; B: $W(\psi_o) = \pi/6$; C: $W(\psi_o) = 0$.

Fig. 4. Director orientation profiles for converging flow, PAA viscosities but varying elastic coefficients. A: all K_{ii} = twice PAA values; B: PAA values; C: all $K_{ii} = 0$.

Fig. 5a. Director orientation profiles in converging flow of PAA as a function of Ericksen number, $W(\psi_o) = \pi/6$. A:E: 84; B: 279; C: 1445; D: 5580.

Fig. 5b. Same as 5a, $W(\psi_o) = 0$. A:E: 4241; B: 885; C: 89.

Fig. 6. Comparison of director orientation distributions in converging flow for PAA and MBBA. A: PAA at $\psi = 0.45$; B: MBBA at $\psi = 0.45$; C: PAA at $\psi = 0.25$; D: MBBA at $\psi = 0.25$.

Fig. 7. Scaled velocity profile for diverging flow of PAA, E: -740. A: $W(\psi_o) = 0$; B: $W(\psi_o) = -\pi/6$; C: Newtonian.

Fig. 8. Director orientation distribution for diverging flow of PAA; E = -740. A: $W(\psi_o) = -\pi/3$; B: $W(\psi_o) = -\pi/6$; C: $W(\psi_o) = 0$.

Fig. 9. Boundary layer thickness as a function of Ericksen number. Full line: numerical solutions; – – – : Eq. (6.12); – • – : Eq. (6.9).

Fig. 10. Effect of radial magnetic field on director orientation in converging flow of PAA. A: $Z^2 = 27$, $E = 870$; B: $Z^2 = 427$, $E = 651$; C: Z^2: 1220, $E = 205$.

Fig. 11. Effect of azimuthal magnetic field on director orientation in converging flow of PAA. A: Z^2: 2862, E: 2548; B: $Z^2 = 1536$, $E = 3136$; C: $Z^2 = 0$ (no field), $E = 4241$.

Fig. 12. Determination of the critical azimuthal field for converging flow of PAA by intersection of the 45^0 line with the curve of $-2\lambda(U(o)$ vs. $1/D$.

Fig. 13. Director orientation distribution for converging flow of PAA near the critical azimuthal field. A: $Z^2 = 155$, $E = 94$ (just prior to transition); B: $Z^2 = 381$, $E = -2.5$ (flow reversal); C: $Z^2 = 315$, $E = 25$ (just after transition).

Fig. 14. Effect of a radial magnetic field on director orientation for diverging flow of PAA. A: $Z^2 = 0$ (no field), $E = -38$; B: $Z^2 = 147$, $E = -84$; C: $Z^2 = 5437$, $E = -4412$.

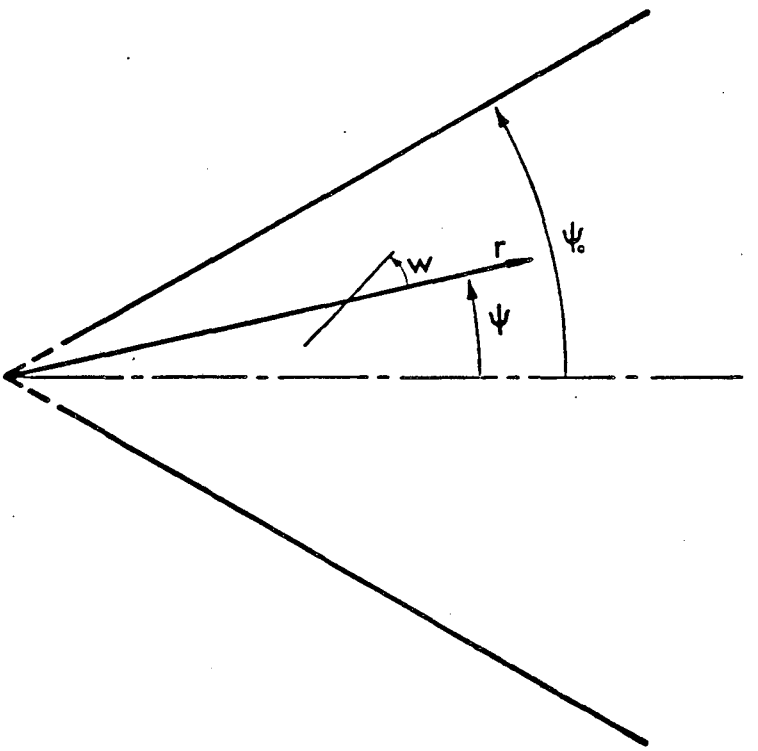

Figure 1

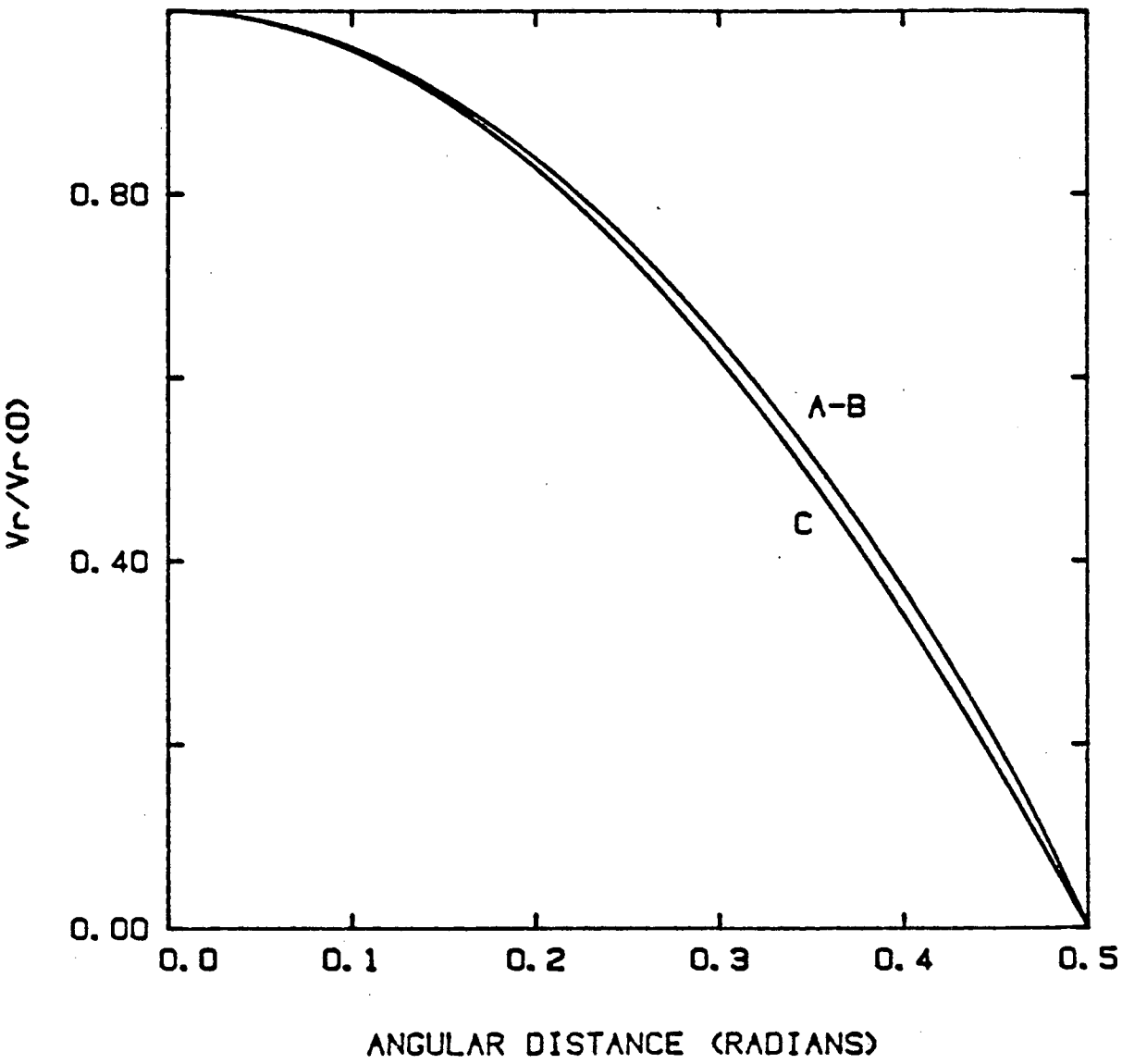
0.80
0.40
0.00
Vr/Vr(0)
A-B
C
0.0
0.1
0.2
0.3
0.4
0.5
ANGULAR DISTANCE (RADIANS)

Figure 2

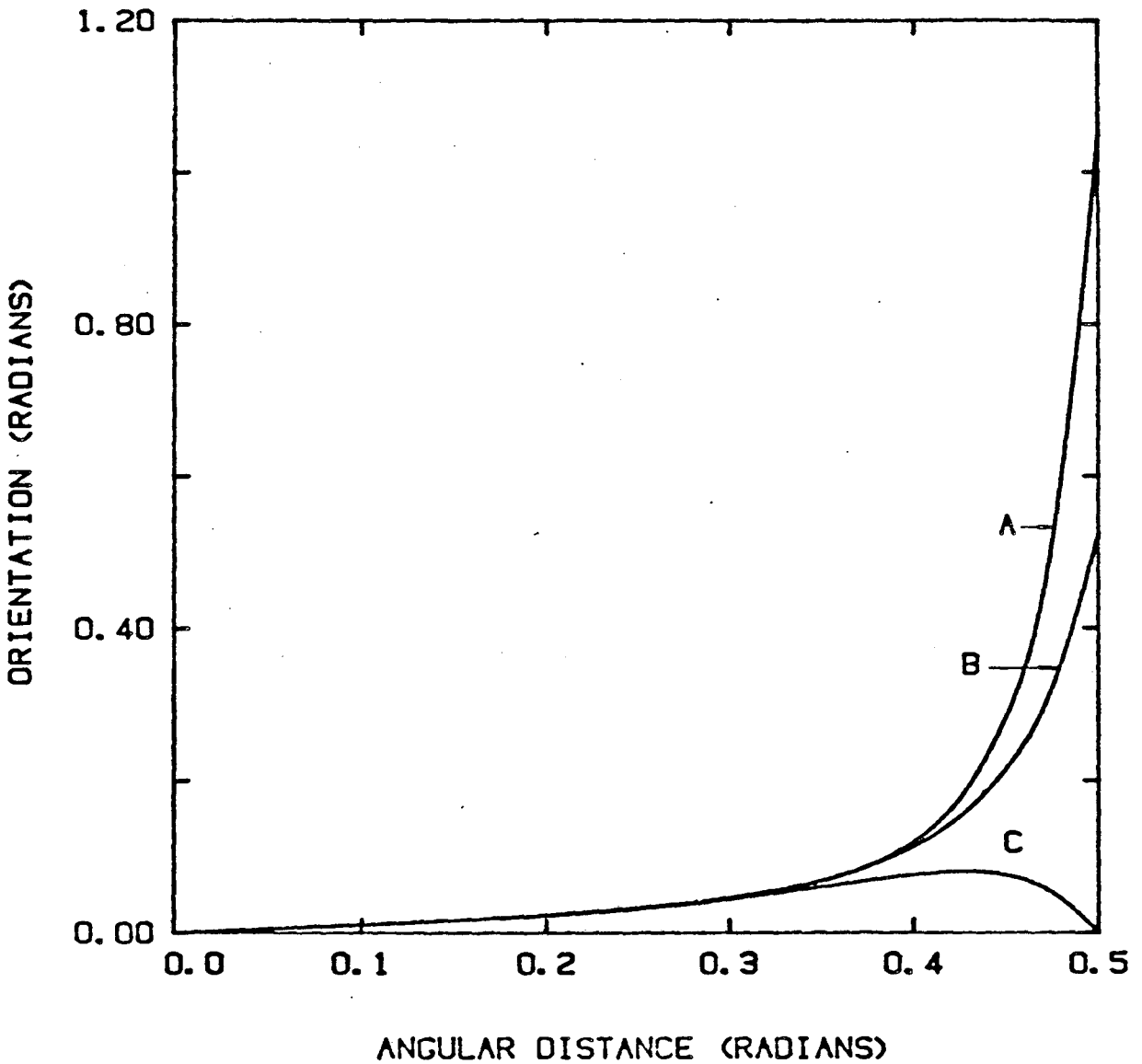
1.20
0.80
0.40
0.00
ORIENTATION (RADIANS)
0.0
0.1
0.2
0.3
0.4
0.5
ANGULAR DISTANCE (RADIANS)
A
B
C

Figure 3

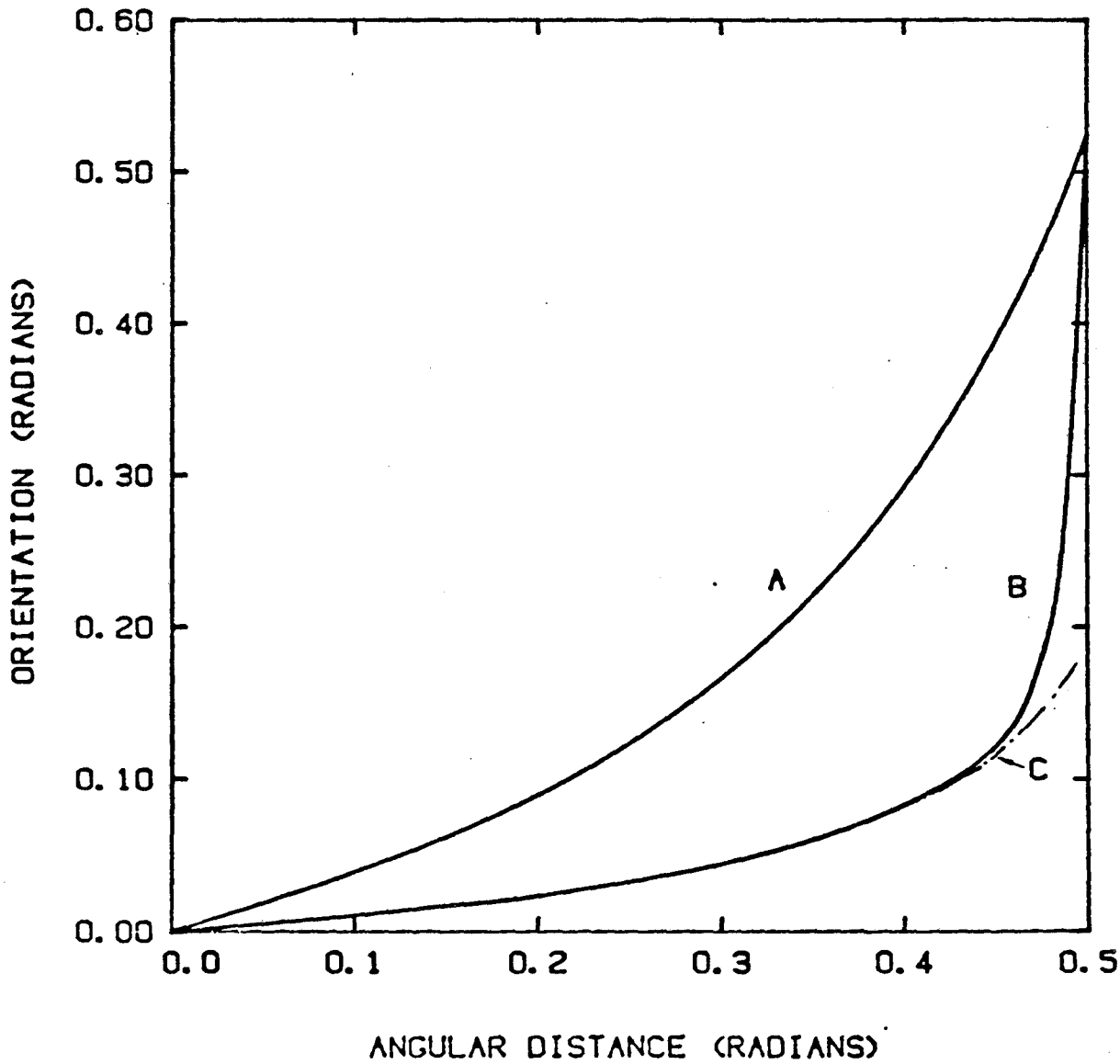
0.60
0.50
0.40
0.30
0.20
0.10
0.00
ORIENTATION (RADIANS)
0.0
0.1
0.2
0.3
0.4
0.5
ANGULAR DISTANCE (RADIANS)
A
B
C

Figure 4

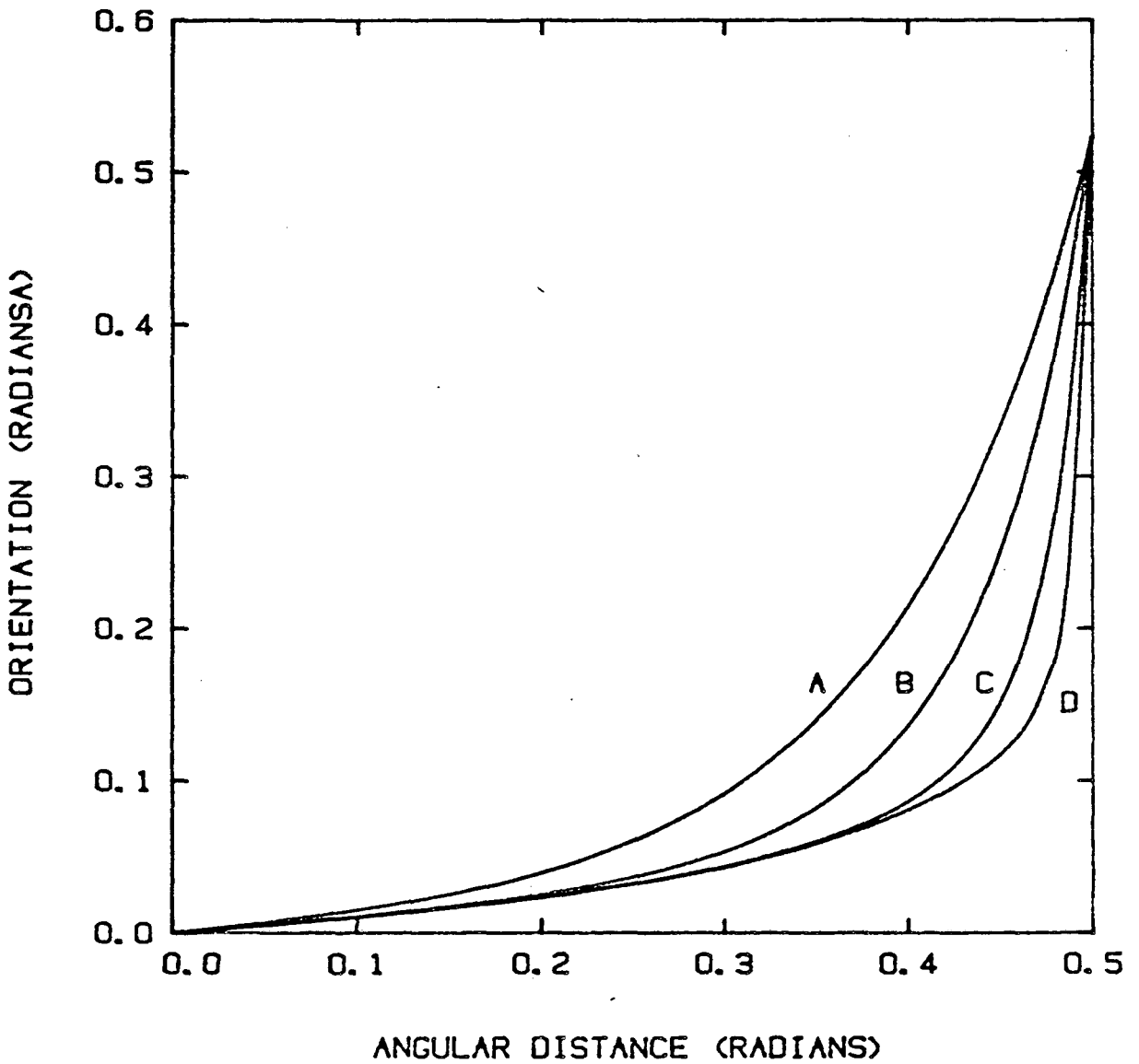
0.6
0.5
0.4
0.3
0.2
0.1
0.0
ORIENTATION (RADIANSA)
A
B
C
D
0.0
0.1
0.2
0.3
0.4
0.5
ANGULAR DISTANCE (RADIANS)

Figure 5a

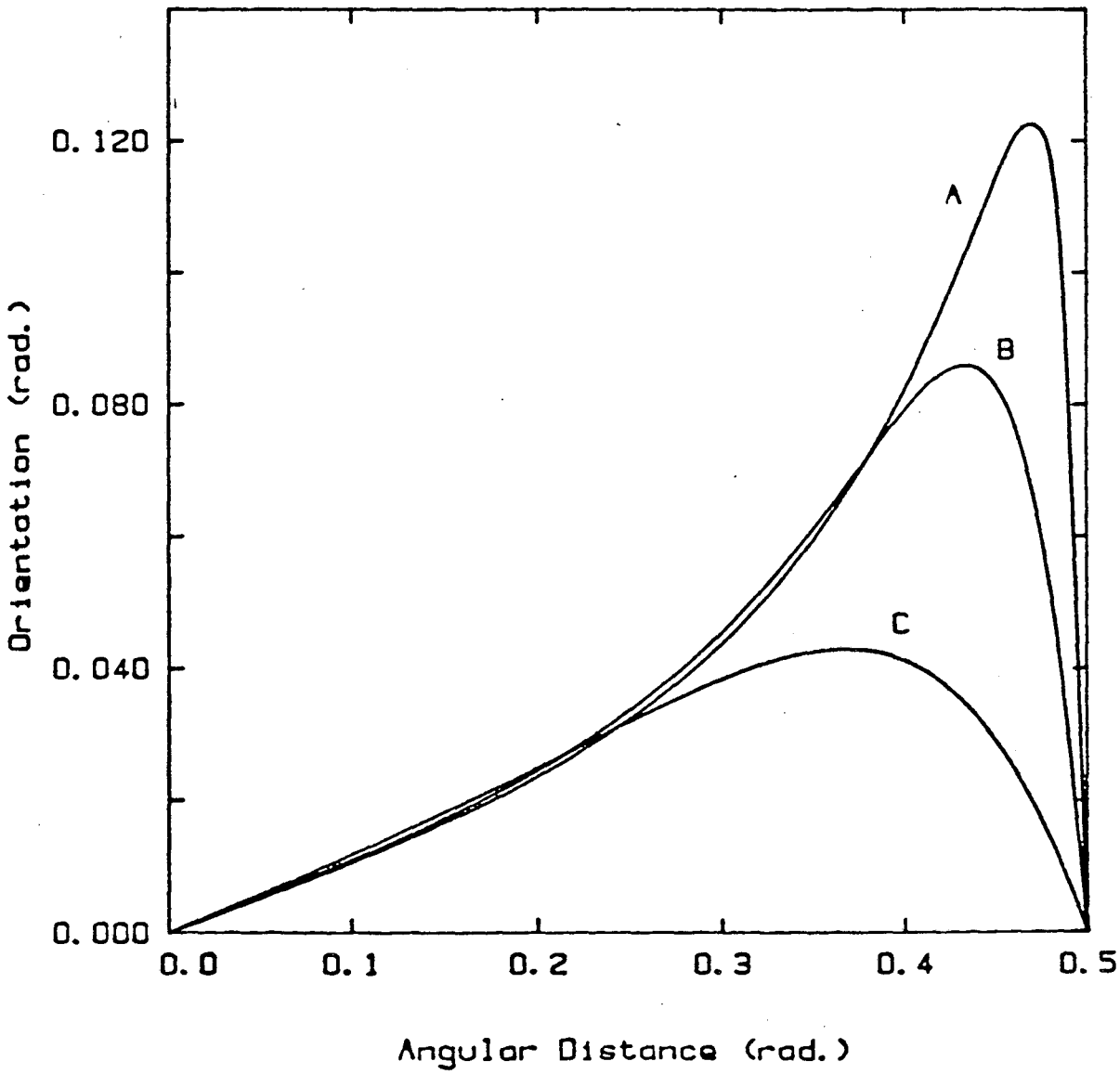
0.120
0.080
0.040
0.000
Orientation (rad.)
0.0
0.1
0.2
0.3
0.4
0.5
Angular Distance (rad.)
A
B
C

Figure 5b

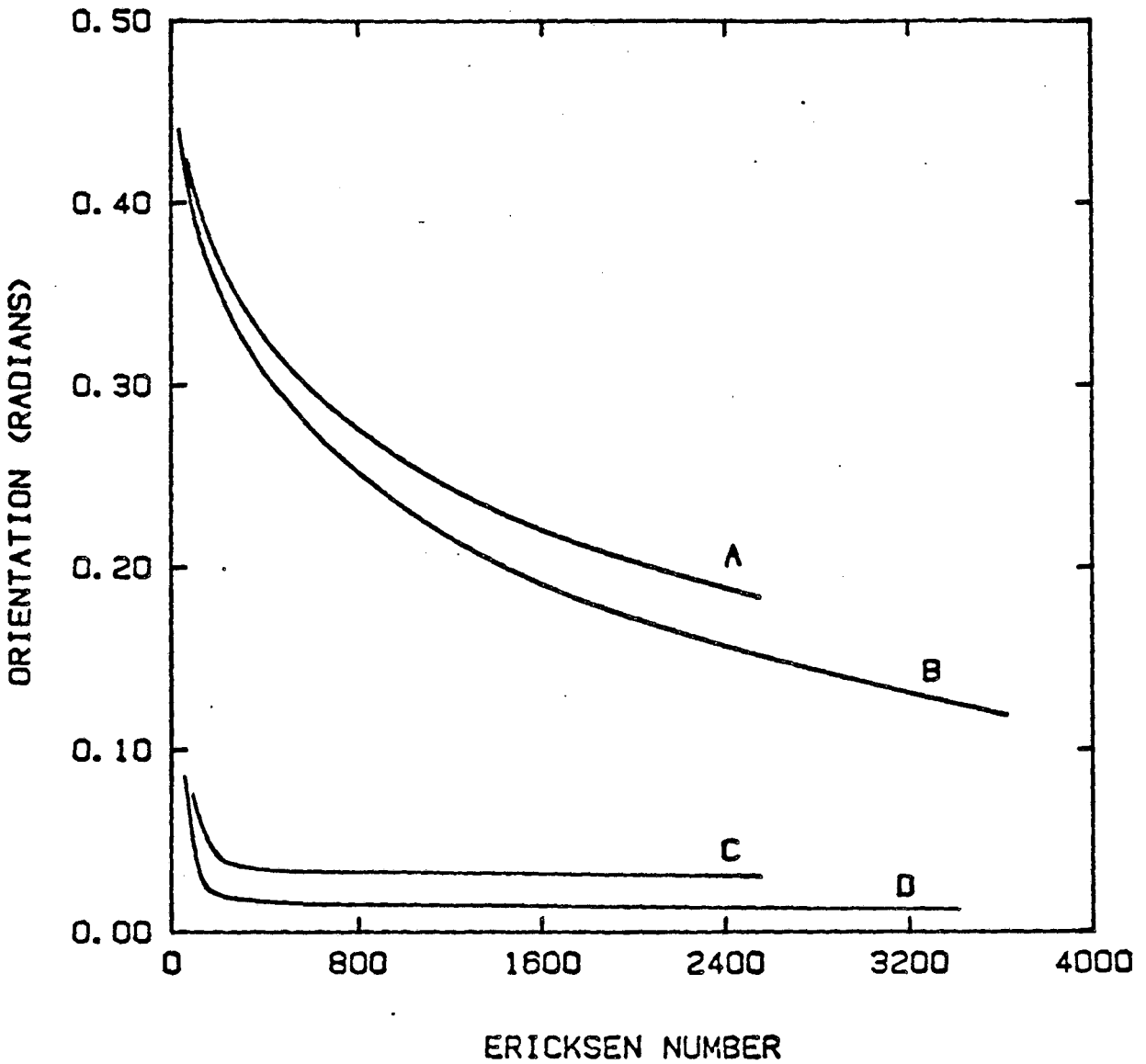
0.50
0.40
0.30
0.20
0.10
0.00
ORIENTATION (RADIANS)
A
B
C
D
0
800
1600
2400
3200
4000
ERICKSEN NUMBER

Figure 6

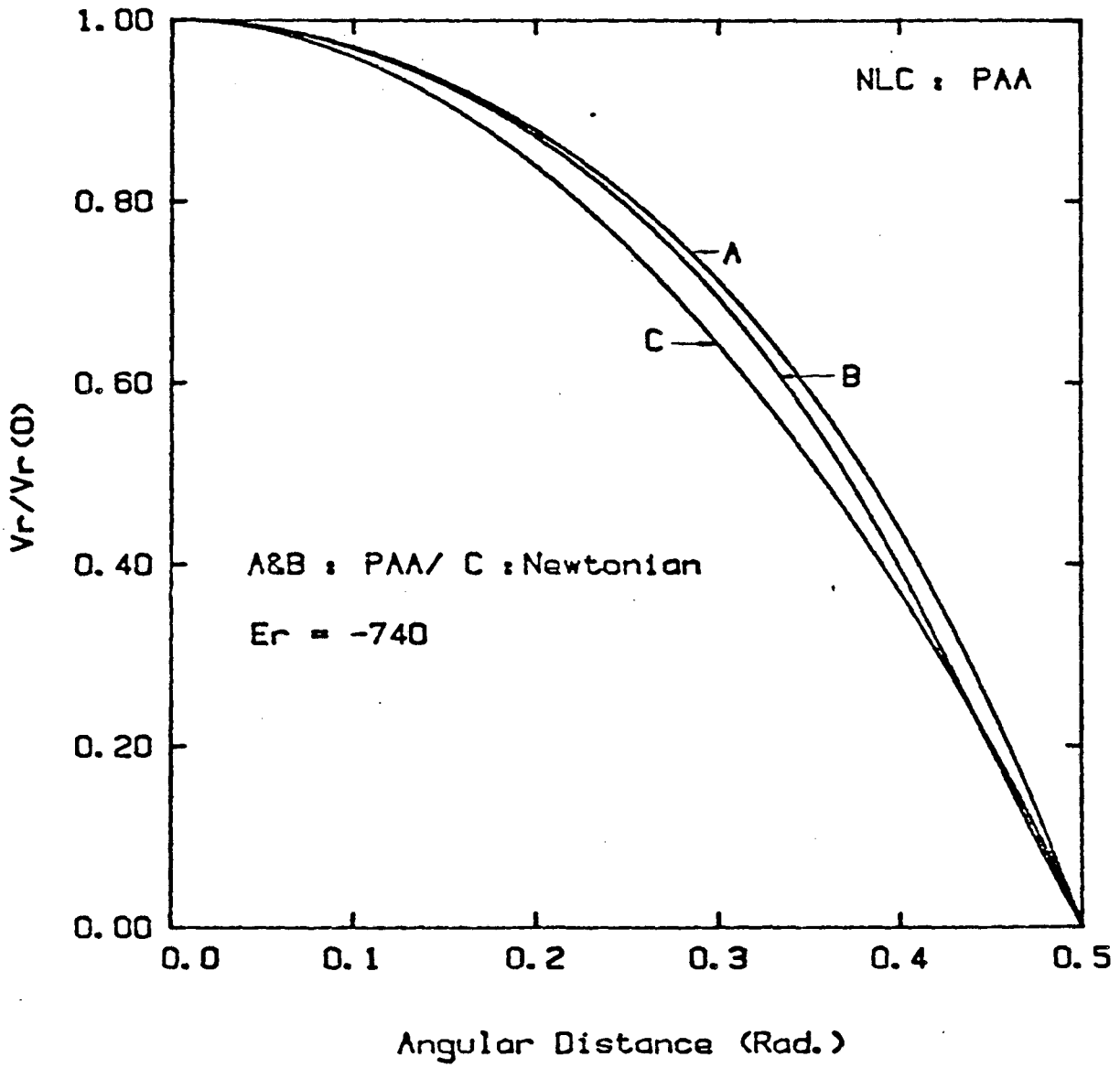
1.00
0.80
0.60
0.40
0.20
0.00
Vr/Vr(0)
NLC : PAA
A
B
C
A&B : PAA/ C : Newtonian
Er = -740
0.0
0.1
0.2
0.3
0.4
0.5
Angular Distance (Rad.)

Figure 7

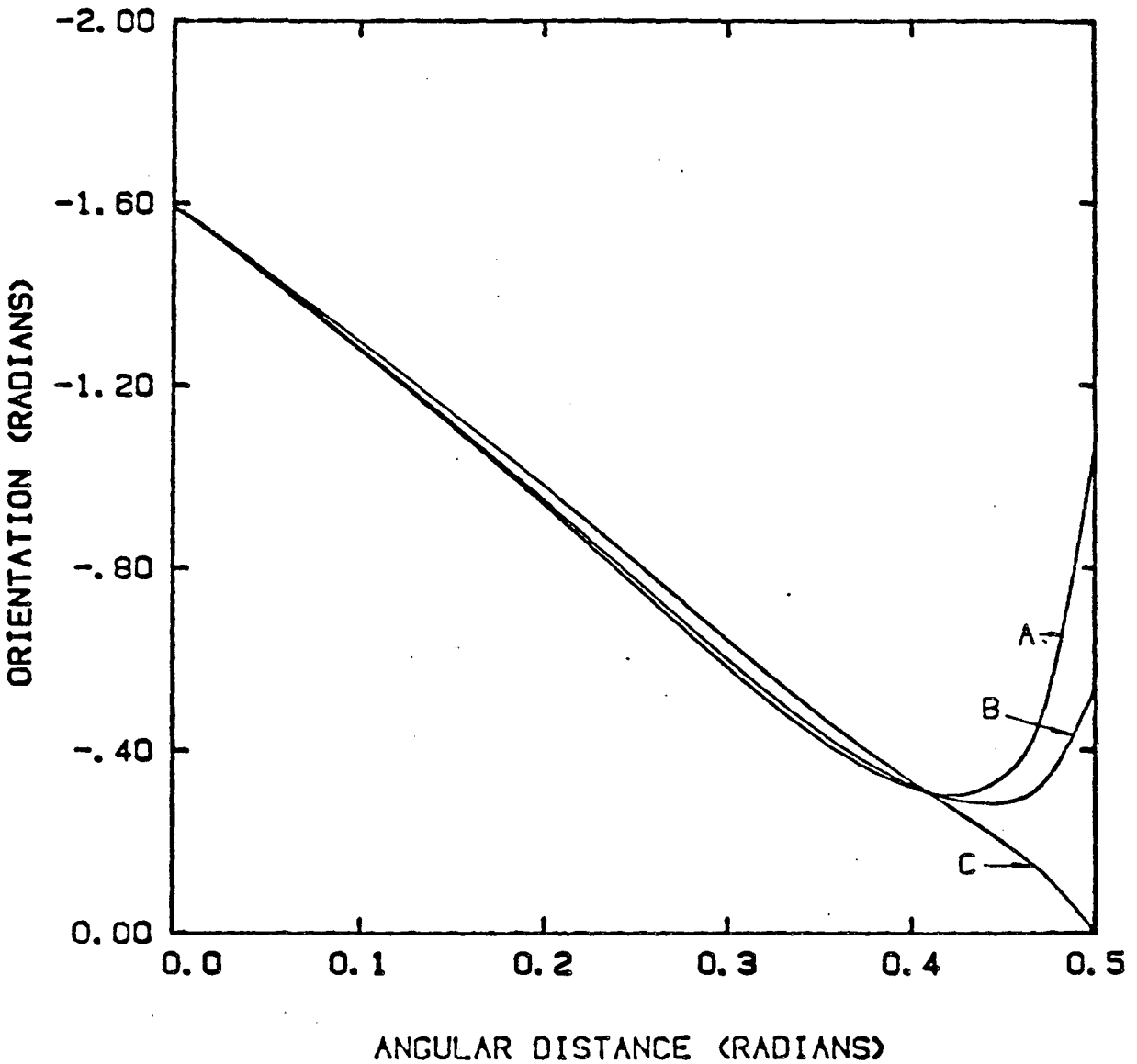
-2.00
-1.60
-1.20
-.80
-.40
0.00
ORIENTATION (RADIANS)
0.0
0.1
0.2
0.3
0.4
0.5
ANGULAR DISTANCE (RADIANS)
A
B
C

Figure 8

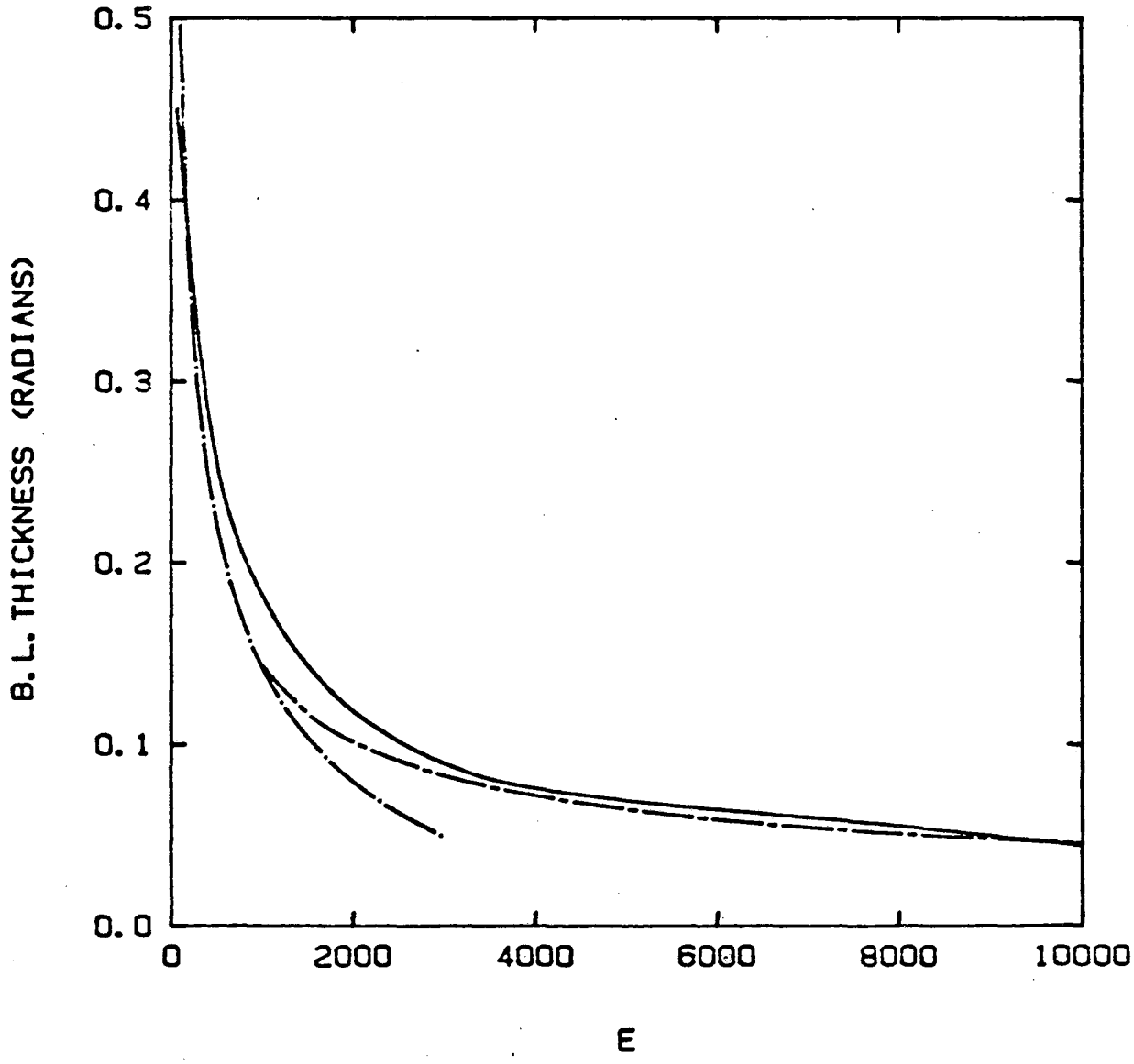
0.5
0.4
0.3
0.2
0.1
0.0
B.L. THICKNESS (RADIANS)
0
2000
4000
6000
8000
10000
E

Figure 9

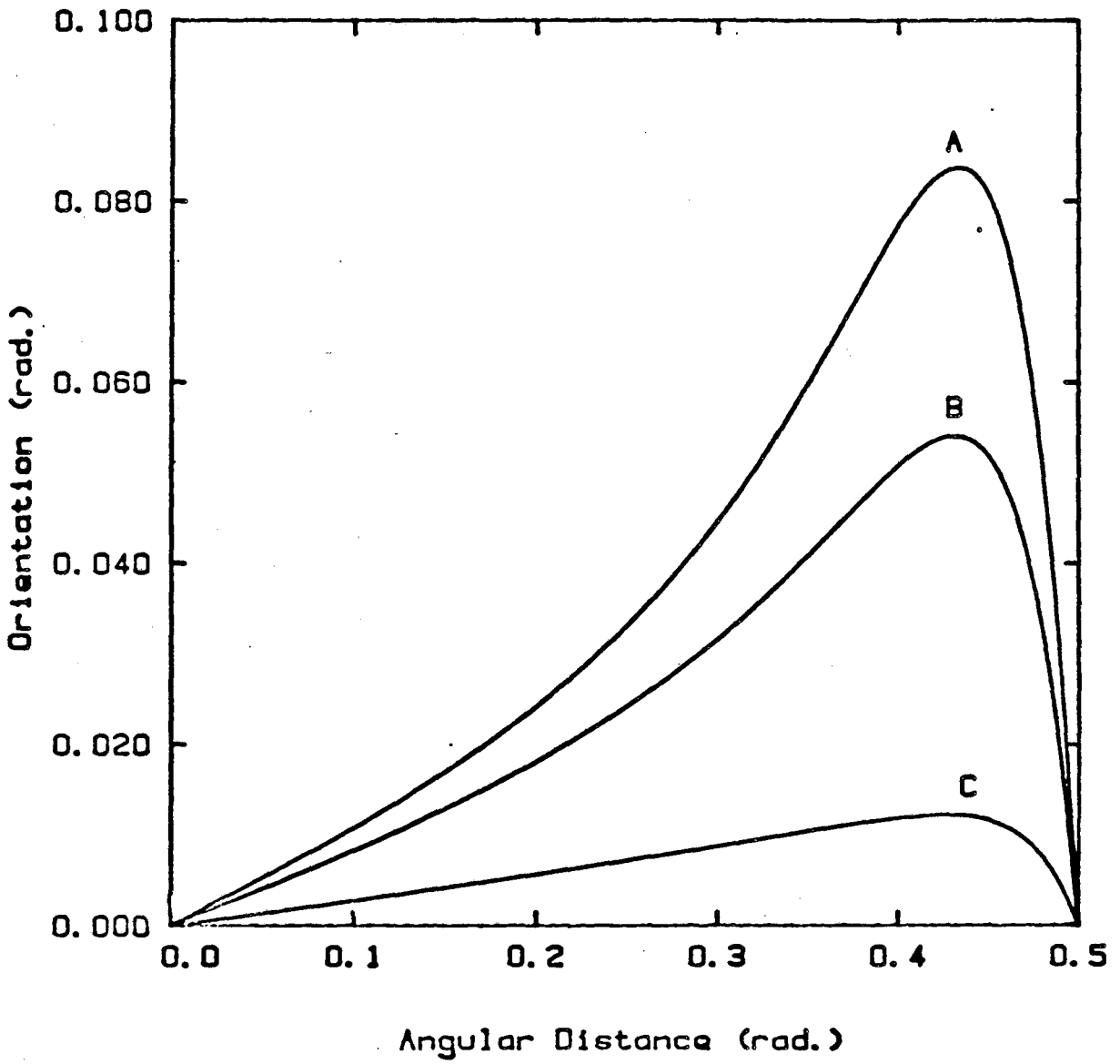
0.100
0.080
0.060
0.040
0.020
0.000
Orientation (rad.)
A
B
C
0.0
0.1
0.2
0.3
0.4
0.5
Angular Distance (rad.)

Figure 10

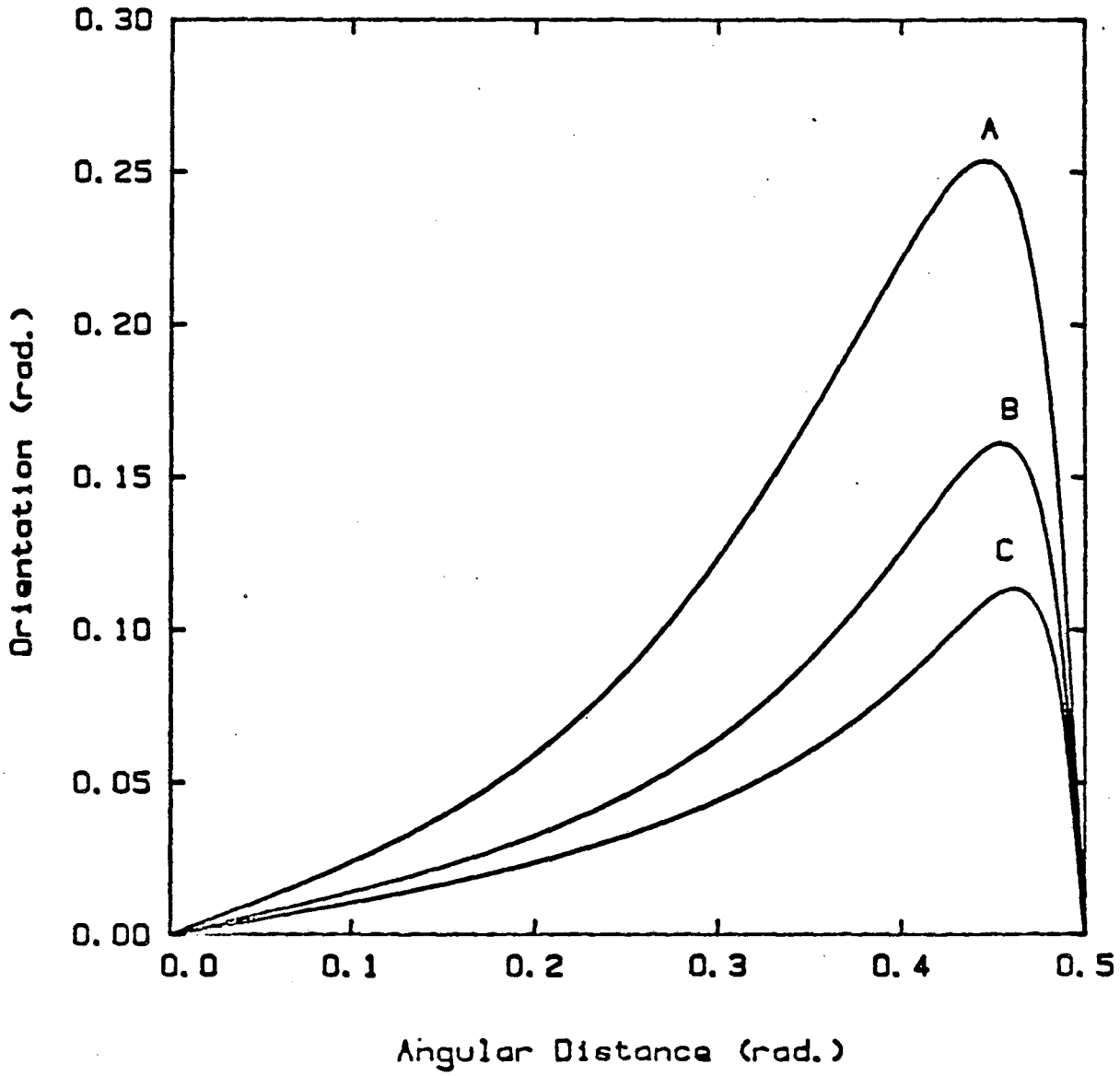
0.30
0.25
0.20
0.15
0.10
0.05
0.00
Orientation (rad.)
A
B
C
0.0
0.1
0.2
0.3
0.4
0.5
Angular Distance (rad.)

Figure 11

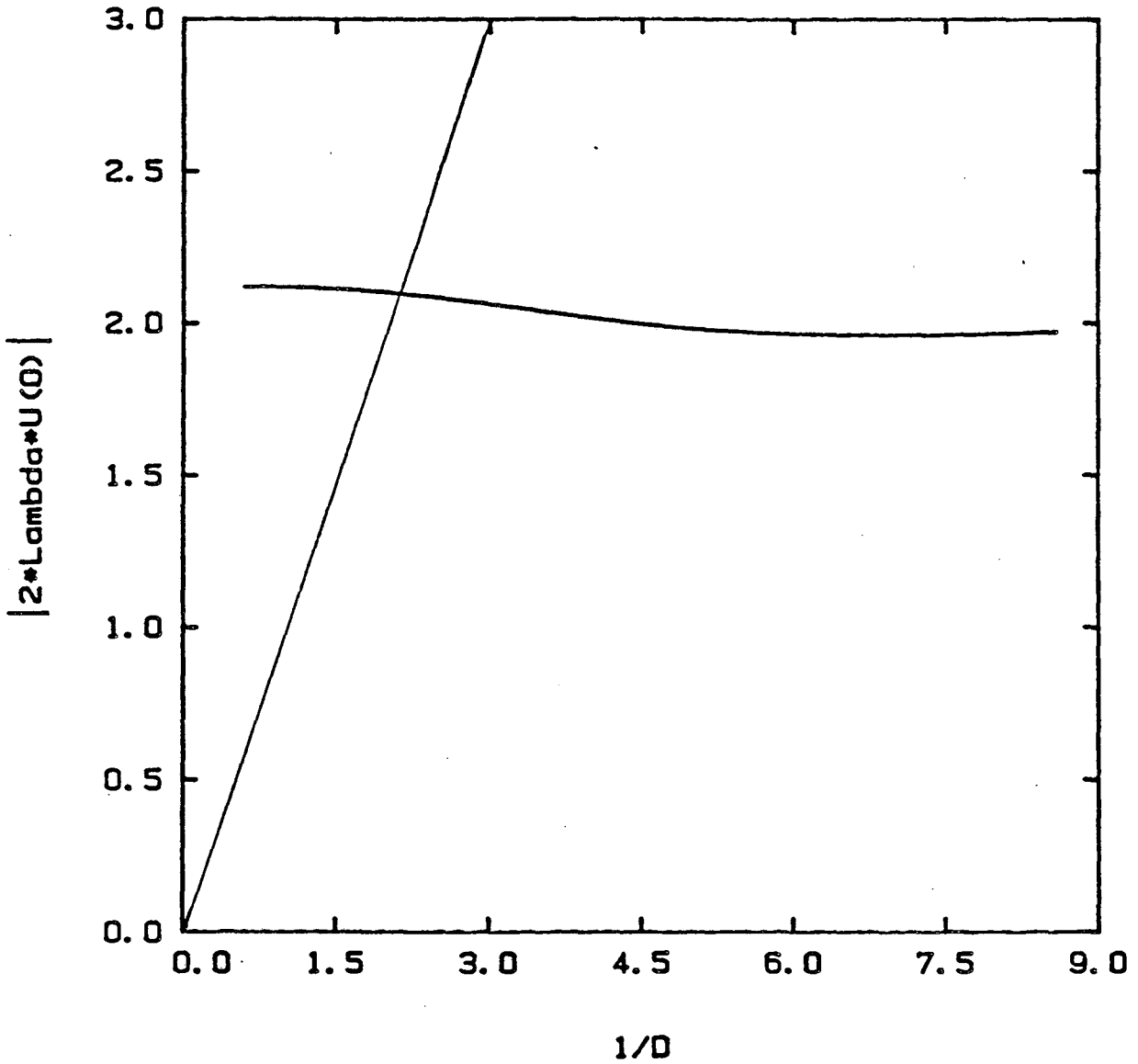

Figure 12

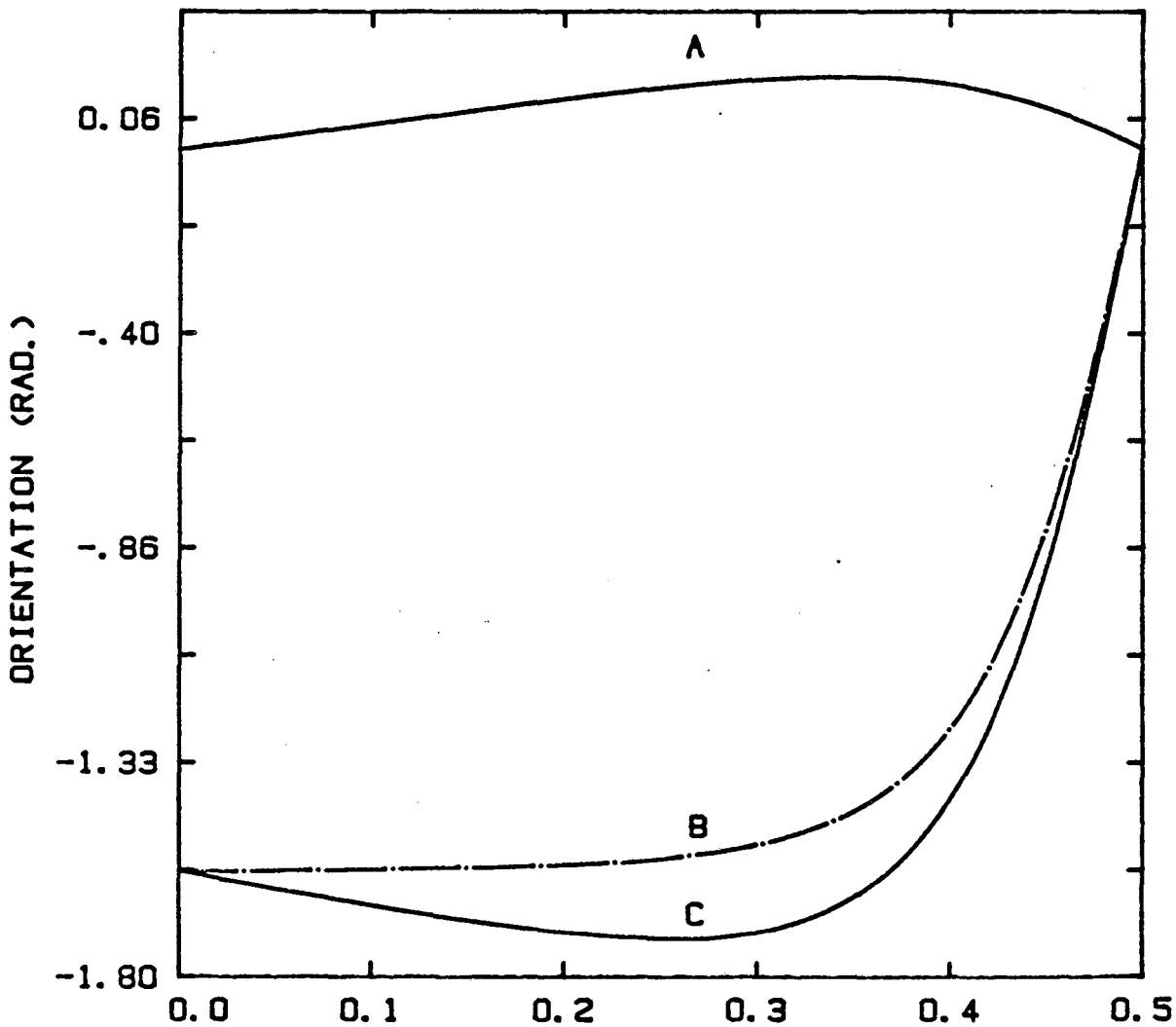

Figure 13

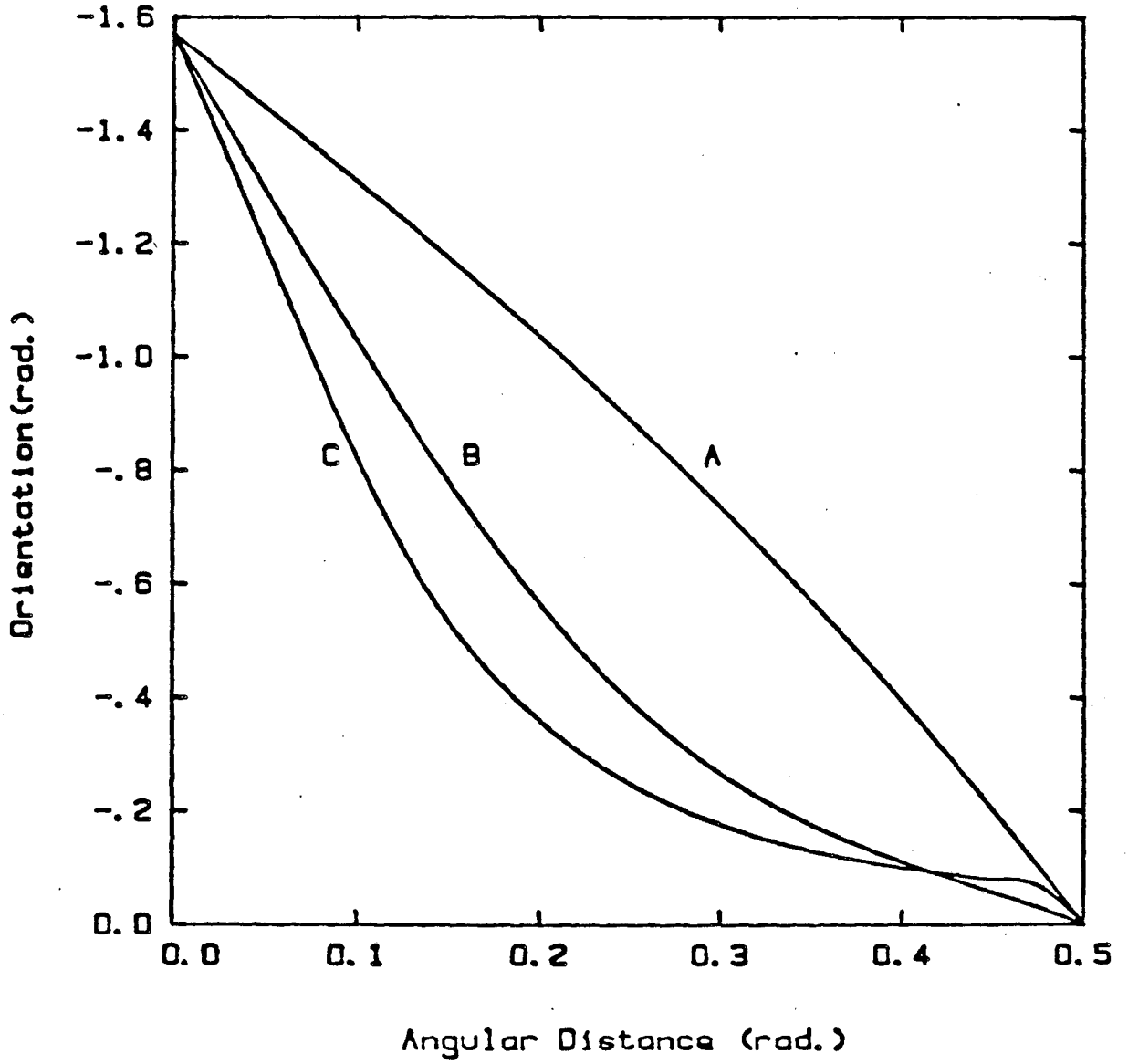
-1.6
-1.4
-1.2
-1.0
-.8
-.6
-.4
-.2
0.0
Orientation (rad.)
C
B
A
0.0
0.1
0.2
0.3
0.4
0.5
Angular Distance (rad.)

Figure 14

LAWRENCE BERKELEY LABORATORY
TECHNICAL INFORMATION DEPARTMENT
UNIVERSITY OF CALIFORNIA
BERKELEY, CALIFORNIA 94720